NASA Technical Paper 3007

August 1990

Buckling and Postbuckling Behavior of Square Compression-Loaded Graphite-Epoxy Plates With Circular Cutouts

Michael P. Nemeth

NASA

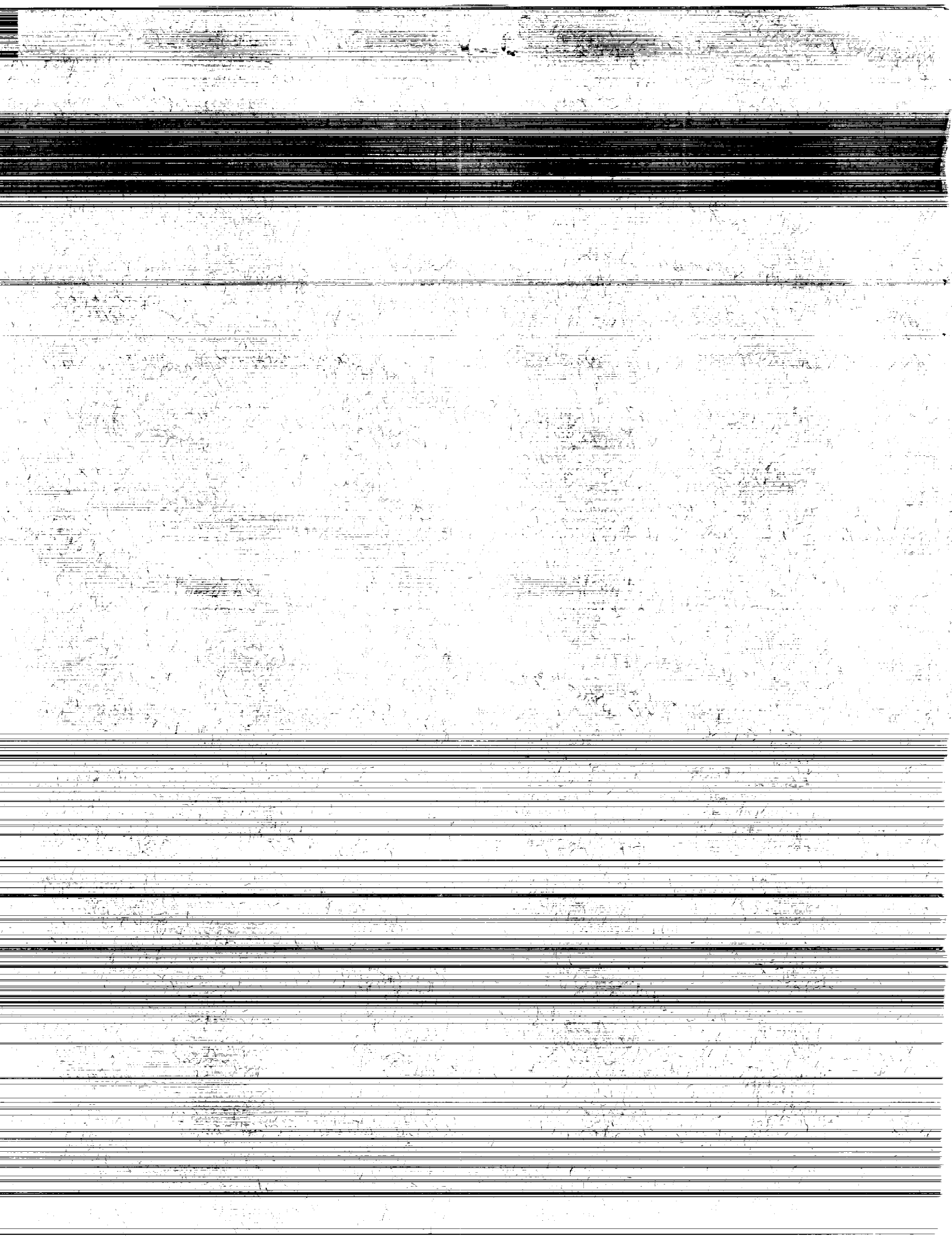

NASA Technical Paper 3007

1990

Buckling and Postbuckling Behavior of Square Compression-Loaded Graphite-Epoxy Plates With Circular Cutouts

Michael P. Nemeth
Langley Research Center
Hampton, Virginia

National Aeronautics and Space Administration
Office of Management
Scientific and Technical Information Division

Summary

An experimental study of the postbuckling behavior of square compression-loaded graphite-epoxy plates and isotropic plates with a central circular cutout is presented. Results are presented for unidirectional $[0_{10}]_s$ and $[90_{10}]_s$ plates, $[(0/90)_5]_s$ plates, and for aluminum plates. Results are also presented for $[(\pm\theta)_6]_s$ angle-ply plates for values of $\theta = 30°$, 45°, and 60°.

The experimental results indicate that the change in axial stiffness of a plate at buckling is strongly dependent upon cutout size and plate orthotropy. The presence of a cutout gives rise to an internal load distribution that changes, sometimes dramatically, as a function of cutout size coupled with the plate orthotropy. In the buckled state, the role of orthotropy becomes more significant, since bending in addition to membrane orthotropy is present. Most of the plates with cutouts exhibited less postbuckling stiffness than the corresponding plate without a cutout, and the postbuckling stiffness decreased with increasing cutout size. However, some of the highly orthotropic plates with cutouts exhibited more postbuckling stiffness than the corresponding plate without a cutout. These results suggest that the complex interaction of cutout size and plate orthotropy on the internal load distribution in plates needs further investigation. These results also suggest the possibility of tailoring the cutout size and the stacking sequence of a composite plate to optimize postbuckling stiffness. An important finding of this experimental study is that plates with large radius cutouts exhibit some postbuckling strength.

The experimental results also indicate that a cutout can influence modal interaction in a plate. Specifically, results are presented that show a plate with a relatively small cutout buckling at a higher load than the corresponding plate without a cutout due to modal interaction. Other results are presented that indicate the presence of nonlinear prebuckling deformations, due to material nonlinearity, in the angle-ply plates with $\theta = 45°$ and 60°. The nonlinear prebuckling deformations are more pronounced in the plates with $\theta = 45°$, and become even more pronounced as the cutout size increases. Results are also presented that show how load-path eccentricity due to improper machining of the test specimens affects the buckling behavior. Some of the plates with cutouts and eccentricity exhibited a snap-through type of buckling behavior.

Introduction

The technical challenges associated with the development of military and civilian aerospace vehicles for the 21st century have identified several key areas that need further development. One important area is the design technology and analysis of large-scale composite structures. The high performance requirements of these structures have led to a search for ways to exploit their tailorability to meet specific mission goals.

An important structural component used in practically all aerospace vehicles is the rectangular plate with a central circular cutout. Cutouts commonly appear in plates as access ports for mechanical and electrical systems or are included to reduce the structural weight in components such as wing ribs and spars. Often during flight, these members experience compression loads, and thus their buckling and postbuckling behavior are important factors that must be considered in their design.

Investigations of the buckling behavior of plates with cutouts have appeared in the technical literature since 1943. A summary of these investigations, for both isotropic and laminated composite plates, is given in reference 1. In-depth parametric studies of the buckling behavior of square and rectangular plates with central circular cutouts are presented in references 1 through 3. Analytical and experimental results are presented in these studies that indicate buckling behavior trends for a wide range of plate parameters. The results and physical insight presented in these references indicate that the buckling behavior of compression-loaded isotropic and orthotropic plates with cutouts is well understood.

Substantially fewer studies on the postbuckling behavior of plates with cutouts are available in the technical literature. Some of the first studies were presented by Yu and Davis in reference 4, by Martin in reference 5, by Yu and Davis in reference 6, and by Ritchie and Rhodes in reference 7. The results presented in references 4 and 6 address the postbuckling collapse of steel beams, columns, and plate girder structures with cutouts in their webs. The results presented in references 5 and 7 focus specifically on square isotropic plates with central circular cutouts. In addition, buckling and postbuckling results are also presented in reference 5 for square laminated composite plates with central circular cutouts.

More recently, selected results for the postbuckling and failure characteristics of compression-loaded rectangular graphite-epoxy plates with central circular cutouts have been presented in reference 8. Additional recent studies of the postbuckling collapse of square isotropic plates with square and circular cutouts are presented in references 9 and 10. A study of the imperfection sensitivity and postbuckling strength of compression-loaded square isotropic

and laminated composite plates with central circular cutouts is presented in reference 11.

Review of the studies presented in references 4 through 11 indicates that the effects of cutout size, plate aspect ratio, and laminate stacking sequence on the postbuckling behavior of plates are still not well understood. This paper examines the behavior of selected isotropic and graphite-epoxy compression-loaded square plates and attempts to establish overall trends indicating the effects of cutout size and plate orthotropy on plate postbuckling behavior. The paper focuses on an experimental study of unidirectional $[0_{10}]_s$ and $[90_{10}]_s$ plates, $[(0/90)_5]_s$ plates, and aluminum plates. These plates represent extreme cases of orthotropy and moderate orthotropy as well as isotropy. Results are also presented for $[(\pm\theta)_6]_s$ angle-ply plates for values of $\theta = 30°$, $45°$, and $60°$.

Symbols

D_{11}, D_{22}	orthotropic plate bending stiffness
d	hole diameter, in. (see fig. 2)
H	nominal plate thickness, in. (see table 8)
K	buckling coefficient, $\frac{P_{cr}W}{\pi^2\sqrt{D_{11}D_{22}}}$
L	plate length, in. (see fig. 2)
P	axial load, lb
P_{cr}	axial load at buckling, lb
P^o_{cr}	axial load at buckling for $d/W = 0$ case, lb (see table 8)
W	plate width, in. (see fig. 2)
Δ	end-shortening, in. (see fig. 2)
Δ^o_{cr}	end-shortening at buckling for $d/W = 0$ case, in. (see table 8)
θ	fiber orientation angle (see fig. 4)
δ	transverse deflection at edge of cutout, in.

Specimens, Apparatus, and Tests

The aluminum specimens tested in this investigation were machined out of 6061-T6 aluminum sheets having a nominal thickness of 0.0625 in. Several thickness measurements were made on each specimen, and the average thickness was determined to be 0.0647 in. Nominal material properties were assumed to include a Young's modulus E of 11.0×10^6 psi and a Poisson's ratio ν of 0.33.

The composite specimens tested in this investigation were fabricated from commercially available 450 K (350°F) cure Hercules AS4/3502 graphite-epoxy preimpregnated tapes. Nominal lamina properties were assumed to include a longitudinal modulus E_1 of 18.5×10^6 psi, a transverse modulus E_2 of 1.6×10^6 psi, an inplane shear modulus G_{12} of 0.832×10^6 psi, a major Poisson's ratio ν_{12} of 0.35, and a nominal ply thickness of 0.005 in. The tapes were laid up to form 20-ply-thick laminates having $[0_{10}]_s$, $[(0/90)_5]_s$, and $[90_{10}]_s$ stacking sequences and to form 24-ply-thick laminates having $[(\pm30)_6]_s$, $[(\pm45)_6]_s$, and $[(\pm60)_6]_s$ stacking sequences.

The laminates were cured in an autoclave with the manufacturer's recommended procedures. After curing, the laminates were ultrasonically C-scanned to assess specimen quality and then machined into test specimens. All specimens were 10 in. long by 10 in. wide, and the loaded edges were machined flat and parallel to permit uniform compressive loading. Central circular cutouts were machined into the aluminum panels with a milling machine and machined into the composite panels with diamond impregnated core drills. The circular cutout diameters ranged from 0 to 6.25 in. One side of each specimen was painted white to reflect light so that a moiré-fringe technique could be used to monitor the out-of-plane deformations. A total of 40 specimens were tested. The specimens have the following designations: A1 through A7 for the aluminum specimens, B1 through B7 for the $[0_{10}]_s$ specimens, C1 through C6 for the $[90_{10}]_s$ specimens, D1 through D7 for the $[(0/90)_5]_s$ specimens, E1 through E5 for the $[(\pm30)_6]_s$ specimens, F1 through F4 for the $[(\pm45)_6]_s$ specimens, and G1 through G4 for the $[(\pm60)_6]_s$ specimens. The cutout sizes for each specimen are given in tables 1 through 7. Several thickness measurements were also made on each composite specimen. The average thickness values were determined to be 0.107 in. for the $[0_{10}]_s$ laminates, 0.106 in. for the $[90_{10}]_s$ laminates, 0.110 in. for the $[(0/90)_5]_s$ laminates, 0.1176 in. for the $[(\pm30)_6]_s$ and $[(\pm60)_6]_s$ laminates, and 0.1307 in. for the $[(\pm45)_6]_s$ laminates.

The specimens were loaded gradually in axial compression with a 300-kip-capacity hydraulic testing machine. The loaded ends of the specimens were clamped by fixtures during testing, and the unloaded edges were simply supported by restraints that prevent the specimen from buckling as a wide column. Most specimens were loaded to approximately twice the buckling load, and then the test was stopped. Some specimens were loaded until failure. A typical specimen mounted in the test fixture is shown in figure 1.

Electrical resistance strain gauges were used to measure strains, and direct-current differential transformers were used to measure axial displacements

and displacements normal to the specimen surface. Electrical signals from the instrumentation and the corresponding applied loads were recorded on magnetic tape at regular time intervals during the tests.

Results and Discussion

Results are presented for several different aluminum and graphite-epoxy plates. First, the methods used to obtain the experimental values of the prebuckling stiffnesses, buckling loads, and initial postbuckling stiffnesses are presented. Results are then presented for the aluminum plates; the $[0_{10}]_s$, $[90_{10}]_s$, and $[(0/90)_5]_s$ specially orthotropic plates; and the $[(\pm 30)_6]_s$, $[(\pm 45)_6]_s$, and $[(\pm 60)_6]_s$ symmetrically laminated angle-ply plates in separate subsections. Failure results are then presented for the specimens that were loaded to failure. After these subsections, results indicating the overall stiffness trends exhibited by the specimens and results indicating the effects of cutout size and plate orthotropy on the distribution of the out-of-plane displacement fields in the specimens are presented. Finally, results showing modal interaction in a plate with a cutout, and results indicating the effects of load-path eccentricity due to improper machining of some of the specimens are presented.

Analysis and Representation of Test Data

To illustrate the postbuckling behavior of plates with cutouts, curves of nondimensional load versus end-shortening and nondimensional load versus transverse deflection are presented in this paper. The curve of nondimensional load versus end-shortening for each specimen was obtained by first performing a least-squares fit of a straight line to the most linear part of the primary branch of the plot of actual load versus end-shortening recorded during the test. With the equation of the line obtained from the least-squares fit of the test data, the prebuckling stiffness was obtained directly, and the initial irregularity in the plot of actual load versus end-shortening, associated with initial slack in the test fixture, was eliminated. The elimination was performed by translating the coordinate system of the plot of actual load versus end-shortening such that the line obtained from the least-squares fit passed through the origin.

In a similar manner, the initial postbuckling stiffness was obtained directly by performing a least-squares fit of a straight line to the most linear part of the secondary branch of the plot of load versus end-shortening recorded during testing. The experimental buckling load and associated end-shortening were then obtained by computing the intersection of the two straight lines fitted to the primary and secondary branches of the test data for load versus end-shortening.

Finally, the curves were nondimensionalized by dividing the load and end-shortening of a given specimen by analytical values of the buckling load P^o_{cr} and end-shortening Δ^o_{cr}, respectively, of the corresponding plate without a cutout. These analytical values were obtained with an in-house computer program for buckling analysis and are based on the nominal material properties given in this paper previously and on nominal plate thicknesses. The nominal plate thicknesses used in the buckling calculations were based on the average values of the measured plate thicknesses previously described. Moreover, the analytical values were based on square-plate geometry, and on a uniaxial loading condition in which two opposite edges of the plate are uniformly displaced toward one another. The loaded edges were assumed to be clamped, and the unloaded edges were assumed to be simply supported. In all the calculations, the buckling load and corresponding end-shortening were based on the 9.5-in. unsupported length between knife edge supports of the test fixture. The nominal thicknesses used in these calculations and the corresponding analytical values are given in table 8.

The results for experimental load versus end-shortening are presented in subsequent sections of the paper by two straight lines obtained from the least-squares fits to the primary and the initial part of the secondary branches of the test data. The intersection of the two straight lines is marked with a solid circular symbol in the figures to denote the experimental buckling load. The nondimensional transverse deflection shown in the figures presented herein was obtained by dividing the actual transverse deflection by the nominal plate thickness that was used to compute P^o_{cr} and Δ^o_{cr}.

Differences between the analytical values and experimental values of the buckling loads and displacements of the plates without cutouts are noted. These differences are attributed to differences between the actual thicknesses of the plates and assumed nominal thickness used in the calculated values, and the assumption of ideal clamped and simply supported boundary conditions in the analysis. The differences between analysis and experiment are also attributed to the difference between the 9.5-in. unsupported length between the ends of the test fixture that was used as the plate width in the buckling calculations and the true plate width of 10 in.

The experimental results for some of the angle-ply laminates exhibited secondary branches of the plots of load versus end-shortening recorded during testing

that were totally nonlinear. This attribute made it difficult to establish the experimental buckling load in the manner previously described. For these cases, the experimental buckling load was estimated from the data for load versus transverse deflection and from strain-gauge data. The initial postbuckling stiffness was taken to be the slope of a line tangent to the secondary branch of the plot of load versus end-shortening and intersecting the straight-line least-squares fit of the primary branch at the estimate of the buckling load. It is important to point out that for these cases, the value of the initial postbuckling stiffness is sensitive to the estimate of the buckling load.

Aluminum Plates

Experimental results were obtained for a square aluminum plate without a cutout, and for square aluminum plates having six different cutout sizes. The cutout size, buckling load, prebuckling stiffness, and postbuckling stiffness of each plate are presented in table 1. Curves for nondimensional load versus end-shortening and nondimensional load versus transverse deflection are presented in figures 2 and 3, respectively.

The results presented in table 1 and figure 2 indicate that the prebuckling stiffnesses of the isotropic plates decrease monotonically with increasing cutout size. This trend is consistent with the fact that an increase in cutout size gives rise to a decrease in the cross-sectional area at the net section of the plate. The maximum decrease in prebuckling stiffness compared with the stiffness of the plate without a cutout is approximately 42 percent for the plate with $d/W = 0.6$.

The results in table 1 also indicate that the buckling loads of the plates decrease at first and then tend to increase with increasing cutout size. Analytical results indicating a similar trend for the buckling loads are presented in reference 1 and suggest that increase in experimental buckling load with increasing cutout size presented herein is not due entirely to scatter in the test data. The buckling mode shapes for all the plates consisted of one half-wave along both their length and width.

Additional results presented in table 1 and figure 2 indicate that the initial postbuckling stiffnesses of the plates decrease monotonically with increasing cutout size. The largest decrease is approximately 43 percent for $d/W = 0.6$. Comparing the prebuckling stiffness with the postbuckling stiffness given in table 1 for each specimen indicates that, as the cutout size increases, the change in axial stiffness due to buckling varies between 35 and 40 percent for the full range of cutout sizes.

The curves for nondimensional load versus transverse deflection shown in figure 3 give an indication of the relative size of the initial imperfection in the geometry of each plate. Moreover, these results give an indication of the nature of the postbuckling deformations near the cutout. For the plates with d/W less than 0.6, the transverse deflection was measured on the top edge of the cutout as indicated in figure 3. For the plate with $d/W = 0.6$, the measurement was made on the right edge of the cutout. The curves shown in this figure cannot be compared directly since the location of the transverse deflection measurement is different for each value of d/W. However, the curves do give some indication of the postbuckling deformation near the cutout, since the transverse deflection measurements for two adjacent cutout sizes (e.g., $d/W = 0.3$ and 0.4) are near one another and the plates possess similar deformation shapes (one half-wave along their length and width). Comparing the relative sizes of the transverse deflections of the specimens with $d/W = 0.5$ and 0.6 suggests that as the cutout size increases, the amount of bending in the top central region of the plate is less than the amount of bending in the right central region of the plate.

Specially Orthotropic Plates

Experimental results were obtained for unidirectional $[0_{10}]_s$, unidirectional $[90_{10}]_s$, and cross-ply $[(0/90)_5]_s$ square plates having up to seven different cutout sizes ranging from $d/W = 0$ to 0.66. The cutout size, buckling load, prebuckling stiffness, and postbuckling stiffness of each $[0_{10}]_s$, $[90_{10}]_s$, and $[(0/90)_5]_s$ plate are presented in tables 2, 3, and 4, respectively. Curves of nondimensional load versus end-shortening and nondimensional load versus transverse deflection are presented in figures 4 and 5, respectively, for the $[0_{10}]_s$ plates; in figures 6 and 7, respectively, for the $[90_{10}]_s$ plates; and in figures 8 and 9, respectively, for the $[(0/90)_5]_s$ plates.

Results for $[0_{10}]_s$ plates. The results presented in table 2 and figure 4 indicate that the prebuckling stiffnesses of the $[0_{10}]_s$ plates decrease monotonically with increasing cutout size, with the exception of the $d/W = 0.32$ case. For this particular case, it was found that the loaded edges of the specimen had not been properly machined. This observation suggests that improper machining of the loaded edges of the test specimen may have produced an edge effect that increased the prebuckling stiffness (see subsequent section entitled "Anomalous behavior"). The maximum decrease in prebuckling stiffness is approximately 74 percent for the plate with $d/W = 0.66$.

The results presented in table 2 also indicate that the buckling loads of the plates decrease monotonically with increasing cutout size. Analytical results showing essentially the same trend are presented in reference 2. The maximum reduction is approximately 33 percent for the plate with $d/W = 0.66$. The buckling mode shapes for all the plates consisted of one half-wave along both the plate lengths and widths.

The results presented in table 2 and figure 4 also indicate that the initial postbuckling stiffnesses of the $[0_{10}]_s$ plates decrease monotonically with increasing cutout size, with the exception of the $d/W = 0.11$ and 0.32 cases. The largest decrease is approximately 24 percent for $d/W = 0.66$. Comparing the prebuckling stiffness with the postbuckling stiffness given in table 2 for each specimen indicates that as the cutout size increases, the change in axial stiffness due to buckling decreases monotonically from approximately a 76-percent stiffness reduction for the plate with $d/W = 0$ to a 31-percent stiffness reduction for the plate with $d/W = 0.66$.

The curves of nondimensional load versus transverse deflection shown in figure 5 indicate that the plates with $d/W = 0.21$ and 0.11 had the largest initial imperfections. In addition, the results in figure 5 suggest that, for the buckled plates, the region adjacent to the cutout (where the transverse deflection was measured) generally becomes more flexible in bending as the cutout size increases.

Results for $[90_{10}]_s$ ***plates.*** The results presented in table 3 and figure 6 indicate that the prebuckling stiffnesses of the $[90_{10}]_s$ plates decrease with increasing cutout size, for the most part, with the exception of the $d/W = 0.42$ case. For this particular case, the prebuckling stiffness was determined to be approximately 16 percent higher than the prebuckling stiffness of the corresponding plate without a cutout. The reduction in prebuckling stiffnesses exhibited by the plates with $d/W < 0.42$ was less than 10 percent of the prebuckling stiffness of the corresponding plate without a cutout. The maximum decrease in prebuckling stiffness is approximately 54 percent for the plates with $d/W = 0.66$. These results suggest that a complex interaction between the plate geometry and the degree of plate orthotropy may be present.

The results presented in table 3 also indicate that the buckling loads of the $[90_{10}]_s$ plates do not decrease monotonically with increasing cutout size. The buckling load of the plate with $d/W = 0.11$ is approximately 9 percent higher than the buckling load of the corresponding plate without a cutout. The lowest buckling load, approximately 30 percent of the buckling load for $d/W = 0$, is exhibited by the plate with $d/W = 0.42$. The plate with $d/W = 0.66$ buckles at a load approximately 18 percent less than the buckling load for the corresponding plate without a cutout. Analytical results showing the same trend are also presented in reference 2 and suggest that the unusual trend exhibited by the plates is not due entirely to scatter in the test data.

In addition, the results presented in table 3 and figure 6 indicate that the initial postbuckling stiffnesses of the plates do not typically decrease with increasing cutout size. In fact, the experimental results indicate initial postbuckling stiffnesses approximately 36 percent larger than the stiffness of the corresponding plate without a cutout for the plate with $d/W = 0.21$, and as high as 56 percent larger for the plate with $d/W = 0.42$. The plate with $d/W = 0.66$ exhibited a stiffness reduction of approximately 43 percent of the initial postbuckling stiffness of the corresponding plate without a cutout. Comparing the prebuckling stiffness with the postbuckling stiffness given in table 3 for each specimen indicates that the change in axial stiffness due to buckling is typically less than that of the $d/W = 0$ case and ranges between 28 and 54 percent of their respective prebuckling stiffnesses.

The curves of nondimensional load versus transverse deflection shown in figure 7 for the $[90_{10}]_s$ plates indicate that the plates with $d/W = 0.42$ and 0.32 exhibit the largest initial imperfections. The results in this figure also suggest that the region adjacent to the cutout in the buckled plates with $d/W > 0.11$ generally becomes more flexible in bending as the cutout size increases. The largest amount of flexibility is exhibited by the plate with $d/W = 0.42$. The results presented in this figure for the plate with $d/W = 0$ indicate that the plate has a relatively large geometric imperfection and deforms out of plane somewhat before moving in the opposite direction to form a nodal line at the center of the plate (where the transverse deflection was measured). The results presented in this figure for the plate with $d/W = 0.11$ indicate that the plate has a very small geometric imperfection and that the central region of the plate deforms initially out of plane as if to form a distinct mode shape and then moves in the opposite direction as if a different mode shape is forming. This observation is directly related to another interesting result presented in table 3 and shown in figure 6 for the plate with $d/W = 0.11$; that is, the plate with $d/W = 0.11$ buckles at a higher load than the corresponding plate without a cutout.

The buckle mode shape for the $[90_{10}]_s$ plate without a cutout consisted of one half-wave in the direction normal to the loading and two half-waves in

the direction parallel to the loading. The buckle mode shape for the $[90_{10}]_s$ plate with $d/W = 0.11$ is shown in figure 10 by the moiré fringe patterns photographed during the test. The fringe pattern for $P/P^o_{cr} = 0.99$ indicates that the plate is beginning to buckle into a mode that lies between the mode observed for the plate with $d/W = 0$ and a mode consisting of one half-wave in each direction. The fringe pattern for $P/P^o_{cr} = 1.14$ shown in figure 10 indicates that as the load increases the plate is moving closer to the mode with two half-waves along the loading direction. The buckling mode shapes for all the plates with $d/W > 0.11$ consisted of one half-wave along both the plate length and width.

To gain insight into this phenomenon, some buckling analyses were performed by using the BUCKO computer code described in reference 12. Analytical results were obtained for $[90_{10}]_s$ plates, based on nominal lamina properties and ply thicknesses; for plate aspect ratios ranging from $L/W = 0.4$ to 2.0; and for cutout sizes of $d/W = 0$ and 0.10. These analytical results are shown in figure 11.

The analytical results shown in figure 11 are the usual festooned curves that relate buckling coefficient K to plate aspect ratio L/W. At the first set of cusps in these curves, the buckle mode changes from one half-wave along the loading direction to two half-waves. The analytical results indicate that the plate with $L/W = 1$ and $d/W = 0.10$ is on the cusp of the intersecting dashed-line curve. This analytical result and the experimental results previously described suggest that a modal interaction was present during the test of the $[90_{10}]_s$ plate with $d/W = 0.11$. Moreover, the resulting interaction gave rise to a slight increase in buckling load.

Results for* $[(0/90)_5]_s$ *plates. The results presented in table 4 and figure 8 indicate that the prebuckling stiffnesses of the $[(0/90)_5]_s$ plates decrease with increasing cutout size, with the exception of the plate with $d/W = 0.42$. This plate exhibits a prebuckling stiffness almost equal to that of the plate with $d/W = 0.32$. The maximum decrease in prebuckling stiffness is approximately 61 percent for the plate with $d/W = 0.66$.

The results presented in table 4 also indicate that the buckling loads of the plates decrease monotonically as d/W increases up to 0.32, and then the buckling loads change very little as d/W increases. The buckling loads of the plate with $d/W = 0.32$ and 0.66 are approximately 11 percent and 5 percent less than the buckling load of the corresponding plate without a cutout, respectively. Analytical results indicating a somewhat similar trend are also presented in reference 2. The buckling mode shapes for all the plates consisted of one half-wave along both the plate length and width.

The results presented in table 4 and figure 8 indicate that the initial postbuckling stiffnesses of the plates decrease monotonically with increasing cutout size. The largest decrease is approximately 51 percent for $d/W = 0.66$. Comparing the prebuckling stiffness to the postbuckling stiffness given in table 4 for each specimen indicates that as the cutout size increases, the change in axial stiffness due to buckling decreases from approximately a 53 percent stiffness reduction for $d/W = 0$ to a 31 percent stiffness reduction for $d/W = 0.32$. The stiffness reduction for $d/W = 0.66$ is approximately 41 percent.

The curves of nondimensional load versus transverse deflection shown in figure 9 for the $[(0/90)_5]_s$ plates indicate that the plates with $d/W = 0.32$ and 0.21 had the largest initial imperfections. The results presented in this figure for the plate with $d/W = 0.66$ indicate that the plate initially deforms in the direction of its geometric imperfection shape and then buckles into a similar mode shape in the opposite direction. This behavior is manifested in figure 8 by the small jump in the curve of load versus end-shortening (similar to what is encountered when a change in buckle mode occurs) near the buckling load for the plate with $d/W = 0.66$.

Symmetrically Laminated Angle-Ply Plates

Experimental results were also obtained for $[(\pm30)_6]_s$, $[(\pm60)_6]_s$, and $[(\pm45)_6]_s$ square plates having up to five different cutout sizes ranging from $d/W = 0$ to 0.66. The cutout size, buckling load, prebuckling stiffness, and postbuckling stiffness of each $[(\pm30)_6]_s$, $[(\pm60)_6]_s$, and $[(\pm45)_6]_s$ plate are presented in tables 5, 6, and 7, respectively. Curves of nondimensional load versus end-shortening and nondimensional load versus transverse deflection are presented in figures 12 and 13, respectively, for the $[(\pm30)_6]_s$ plates; in figures 14 and 15, respectively, for the $[(\pm60)_6]_s$ plates; and in figures 16 and 17, respectively, for the $[(\pm45)_6]_s$ plates.

Results for* $[(\pm30)_6]_s$ *plates. The results presented in table 5 and figure 12 indicate that the prebuckling stiffnesses of the $[(\pm30)_6]_s$ plates decrease monotonically with increasing cutout size. The maximum decrease in prebuckling stiffness is approximately 54 percent for the plate with $d/W = 0.66$.

The results presented in table 5 also indicate that the buckling loads of the plates decrease monotonically with increasing cutout size up to $d/W = 0.60$. The buckling load of the plate with $d/W = 0.60$ is

approximately 16 percent less than the buckling load of the corresponding plate without a cutout. The plate with $d/W = 0.66$ exhibits a buckling load approximately 13 percent less than the buckling load of the corresponding plate without a cutout. Analytical results that indicate a somewhat similar trend are presented in reference 3. The buckling mode shapes for all the plates consisted of one half-wave along both their length and width.

The results presented in table 5 and figure 12 indicate that the initial postbuckling stiffnesses of the plates with $d/W = 0.11$ and 0.32 are approximately 4 percent higher than the postbuckling stiffness of the plate with $d/W = 0$. The plates with $d/W = 0.60$ and 0.66 exhibit initial postbuckling stiffnesses that are, respectively, approximately 16 percent and 27 percent less than the stiffness of the corresponding plate without a cutout. Comparing the prebuckling stiffness with the postbuckling stiffness given in table 5 for each plate indicates that, as the cutout size increases, the change in axial stiffness due to buckling decreases monotonically from approximately a 66-percent stiffness reduction for $d/W = 0$ to a 46-percent stiffness reduction for $d/W = 0.66$.

The curves of nondimensional load versus transverse deflection shown in figure 13 indicate that the plates with $d/W = 0.11$ and 0 had the largest initial imperfections. The results also suggest that the region adjacent to the cutout in the buckled plates with $d/W \leq 0.32$ becomes more flexible in bending as the cutout size increases. The results presented in this figure for the plates with $d/W = 0.60$ and 0.66 indicate that the plates failed at loads much lower in the postbuckling range than the other plates.

Results for $[(\pm 60)_6]_s$ ***plates.*** The results presented in table 6 and figure 14 indicate that the prebuckling stiffnesses of the $[(\pm 60)_6]_s$ plates decrease monotonically with increasing cutout size. The maximum decrease in prebuckling stiffness is approximately 60 to 69 percent for the plate with $d/W = 0.66$. The curve of nondimensional load versus end-shortening shown in figure 14 for the plate with $d/W = 0.66$ exhibits a nonlinear prebuckling path. Neglecting the nonlinearity gives a prebuckling stiffness reduction due to the cutout of approximately 60 percent, whereas including the nonlinearity accounts for another 9-percent reduction in stiffness. Because of the nonlinear path, the buckling load was estimated with the corresponding curve of nondimensional load versus transverse deflection presented in figure 15. At the buckling load, the secondary branch of the curve of load versus end-shortening is linear. Strain-gauge data (for back-to-back pairs of gauges located near the edge of the cutout) recorded during testing of the plate with $d/W = 0.66$ corroborated the presence of material nonlinearity. This fact is illustrated in figure 18 by the nonlinear shape of the initial part of the curves giving nondimensional load versus axial strain. The strain-gauge data for the plates with the smaller cutout sizes showed no indication of material nonlinearity prior to buckling.

The results presented in table 6 also indicate that the buckling loads of the plates decrease monotonically with increasing cutout size up to $d/W = 0.32$. The buckling load of the plate with $d/W = 0.32$ is approximately 16 percent less than the buckling load of the corresponding plate without a cutout. The plate with $d/W = 0.66$ exhibits a buckling load 23 percent greater than the buckling load of the corresponding plate without a cutout. These buckling loads exhibit a trend that is similar to the analytically obtained buckling loads presented in reference 3. The buckling mode shapes for all the plates consisted of one half-wave along both the plate length and width.

The results presented in tables 6 and figure 14 indicate that the initial postbuckling stiffnesses of the plates decrease with increasing cutout size. The largest reduction in stiffness is exhibited by the plate with $d/W = 0.66$, and is approximately 74 percent of the stiffness of the corresponding plate without a cutout. The plates with $d/W = 0$ and 0.11 also exhibit a change in buckle pattern from one half-wave along the loading direction to two half-waves along the loading direction at approximately $P/P_{cr}^o = 1.4$. Associated with these changes in buckle pattern are additional reductions in postbuckling stiffness of 26 and 34 percent of the corresponding prebuckling stiffnesses for the plates with $d/W = 0$ and 0.11, respectively. Comparing the prebuckling stiffness with the postbuckling stiffness given in table 6 for each specimen with $d/W < 0.66$ indicates that as the cutout size increases, the axial stiffness due to initial buckling decreases about 33 to 39 percent. The plate with $d/W = 0.66$ exhibits a stiffness reduction (including the effects of material nonlinearity) of approximately 60 percent.

The curves of nondimensional load versus transverse deflection shown in figure 15 suggest that the region adjacent to the cutout (where the displacement was measured) becomes more flexible in bending as the cutout size increases for all cutout sizes except $d/W = 0.66$. The results in this figure also show a change in buckle pattern for the plates with $d/W = 0$ and 0.11 at approximately $P/P_{cr}^o = 1.4$.

Results for $[(\pm 45)_6]_s$ ***plates.*** The results presented in table 7 and figure 16 indicate that the prebuckling stiffnesses of the $[(\pm 45)_6]_s$ plates

decrease monotonically with increasing cutout size. The maximum decrease in prebuckling stiffness is approximately 62 to 88 percent for the plate with $d/W = 0.66$. The curve of nondimensional load versus end-shortening shown in figure 16 for the plate with $d/W = 0.66$ exhibits a substantial nonlinear prebuckling path. Neglecting the nonlinearity gives a prebuckling stiffness reduction due to the cutout of approximately 62 percent, whereas including the nonlinearity accounts for another 26-percent reduction in stiffness.

Because of the nonlinear prebuckling path of the plate with $d/W = 0.66$, the buckling load was estimated with the corresponding curve of nondimensional load versus transverse deflection presented in figure 17. At the buckling load, the secondary branch of the curve of load versus end-shortening is not linear like that of the $[(\pm 60)_6]_s$ plate with $d/W = 0.66$. Placing a tangent line through the buckling load indicates that the initial postbuckling stiffness and the prebuckling stiffness just prior to buckling are the same. This observation suggests that significant nonlinear material behavior was present during buckling. Strain-gauge data (from back-to-back pairs of gauges located near the edge of the cutout) recorded during testing of the $[(\pm 45)_6]_s$ plates indicate the presence of very small amounts of material nonlinearity in the plates with $d/W < 0.66$. These small amounts of material nonlinearity account for the shape of the curves of nondimensional load versus end-shortening shown in figure 16; that is, the curves start out linear and then become substantially nonlinear just after buckling.

The results presented in table 7 also indicate that the buckling loads of the $[(\pm 45)_6]_s$ plates decrease monotonically with increasing cutout size up to $d/W = 0.32$. The buckling loads of the plate with $d/W = 0.32$ and 0.66 are approximately 14 percent less and 14 percent greater, respectively, than the buckling load of the corresponding plate without a cutout. For all the plates, the buckling load was estimated from the appropriate curve of load versus transverse deflection and associated strain-gauge data due to the rapid onset of nonlinear behavior immediately after buckling. The buckling mode shapes for all the plates consisted of one half-wave along both the plate length and width.

The results presented in tables 7 and figure 16 indicate that the initial postbuckling stiffnesses of the plates decrease with increasing cutout size. The largest reduction in stiffness is exhibited by the plate with $d/W = 0.66$ and is approximately 73 percent (including substantial material nonlinearity) of the stiffness of the corresponding plate without a cutout. Comparing the prebuckling stiffness to the postbuckling stiffness given in table 7 for each $[(\pm 45)_6]_s$ plate with $d/W < 0.66$ indicates that as the cutout size increases, the reduction in axial stiffness due to initial buckling is around 45 to 55 percent. The plate with $d/W = 0.66$ exhibits a stiffness reduction of approximately 68 percent that includes the effects of material nonlinearity. An important point to note is that the postbuckling stiffness presented herein for each specimen is dependent upon the estimate of the buckling load due to the nonlinear shape of the curves of nondimensional load versus end-shortening.

The curves of nondimensional load versus transverse deflection shown in figure 17 for the $[(\pm 45)_6]_s$ plates with $d/W < 0.66$ indicate that the region adjacent to the cutout (where the displacement was measured) of the buckled plates becomes more flexible in bending as the cutout size increases. The results presented in this figure for the plate with $d/W = 0.32$ indicate that the plate initially deforms in the direction of its geometric imperfection shape and then buckles into a similar mode shape in the opposite direction. However, no indication of this behavior is given by the corresponding curve of load versus end-shortening. The plate with $d/W = 0.66$ failed before getting very far into the postbuckling range.

Failure Tests

Most of the specimens tested in the experimental study described in this paper were loaded gradually to approximately twice their buckling loads. However, some of the specimens were loaded to failure. The particular specimens loaded to failure, their failure loads, and average axial strains at failure are listed in table 9. The average strains recorded in table 9 are obtained by dividing the end-shortening at failure by the true 10-in. length of the plates.

Three $[90_{10}]_s$ plates with ratios of cutout diameter to plate width d/W of 0.32, 0.42, and 0.66 were loaded to failure. The plate with $d/W = 0.32$ failed at the highest load. The plates with $d/W = 0.42$ and 0.66 failed at loads approximately 19 percent and 15 percent less, respectively, than the failure load of the plate with $d/W = 0.32$. Similarly, the plates with $d/W = 0.42$ and 0.66 failed at average strains approximately 40 percent smaller and 17 times larger, respectively, than the failure strain of the plate with $d/W = 0.32$. In all cases, the $[90_{10}]_s$ specimens failed at the net section of the plate, along the fibers in a matrix failure mode. The curves of nondimensional load versus transverse deflection presented in figure 7 for the $[90_{10}]_s$ plates with $d/W = 0.42$ and 0.66 show an abrupt change in bending stiffness near the cutout that is associated with the onset of matrix cracking. Moreover, the curves shown in figure 7 indicate that all three of

the plates failed at roughly the same magnitudes of transverse deflection.

Two $[(\pm 30)_6]_s$ plates—$d/W = 0.60$ and 0.66—were loaded to failure. The failure loads and average failure strains for the two plates are nearly the same. The plate with $d/W = 0.60$ failed along a line that is parallel to the $+30°$ fibers and runs from the edge of the cutout at the net section to the unloaded edge of the plate. The specimen appeared to have a clean break of the $-30°$ fibers along the failure line just described. The plate with $d/W = 0.66$ failed along a line that is parallel to the $+30°$ fibers and runs from the edge of the cutout to the corner of the plate. This specimen also appeared to have a clean break of the $-30°$ fibers along the failure line just described but did not intersect the cutout at the net section.

One $[(\pm 60)_6]_s$ plate—$d/W = 0.66$—was loaded to failure. The failure load of the $[(\pm 60)_6]_s$ plate was approximately 29 percent less than the failure load of the $[(\pm 30)_6]_s$ plate. However, the average failure strain of the $[(\pm 60)_6]_s$ plate was approximately 3.3 times that of the $[(\pm 30)_6]_s$ plate. In the $[(\pm 60)_6]_s$ plate, the failure appeared to be due to delaminations that started at the unloaded edges of the plate near the net section and propagated to the free edge of the cutout. The delaminations also appeared to propagate along the $+60°$ fiber direction.

One $[(\pm 45)_6]_s$ plate—$d/W = 0.66$—was also loaded to failure. The failure load of the $[(\pm 45)_6]_s$ plate was approximately 4 percent higher than the failure load of the $[(\pm 30)_6]_s$ plate, and the average failure strain of the $[(\pm 45)_6]_s$ plate was approximately 3.6 times larger than that of the $[(\pm 30)_6]_s$ plate. In the $[(\pm 45)_6]_s$ plate, the failure also appeared to be due to delaminations that started at the unloaded edges of the plate near the net section and propagated to the free edge of the cutout. The delaminations also appeared to propagate along the $+45°$ fiber direction.

Discussion of Results

Overall stiffness trends. The experimental results presented in this paper include a wide range of cutout sizes and a broad spectrum of plate orthotropy (in addition to plate isotropy). Only one specimen was tested for each combination of cutout size and plate orthotropy. Due to the limited amount of testing on each specimen type, the degree of scatter in the experimental data is not well-known. However, the experimental data presented in this paper are useful in identifying overall trends exhibited by each family of plates studied. To indicate the overall trends, results showing the reduction in prebuckling stiffness due to cutouts, results showing the change in postbuckling stiffness due to cutouts, and results showing the change in axial stiffness the plates experience in going from an unbuckled state to a buckled state are presented in tables 10, 11, and 12, respectively, for all 40 specimens tested.

The results presented in table 10 indicate the reduction in axial stiffness prior to buckling with respect to the prebuckling stiffness of the corresponding plate without a cutout as a function of inplane plate orthotropy. The results presented in this table indicate a complex interaction between cutout size and plate orthotropy on the stiffness reduction. For example, the $[0_{10}]_s$ plates lose a substantial amount of inplane stiffness (approximately 27 percent) when small cutouts are present, whereas the $[90_{10}]_s$ and $[(\pm 30)_6]_s$ plates retain a substantial amount of stiffness (approximately 88 percent) until d/W becomes greater than 0.32. The largest stiffness reductions are exhibited by the $[0_{10}]_s$ and $[(0/90)_5]_s$ plates for the full range of cutout sizes. The smallest stiffness reductions are exhibited by the $[90_{10}]_s$ plates for most of the cutout sizes. In all cases, the reduction in axial stiffness due to the cutout is generally not equal to the reduction in cross-sectional area at the net section of the plate.

The results presented in table 11 indicate the reduction in initial postbuckling stiffness, with respect to the initial postbuckling stiffness of the corresponding plate without a cutout, as a function of cutout size and plate orthotropy (inplane and bending orthotropy). These results also indicate a complex interaction between cutout size and plate orthotropy that influences the change in postbuckling stiffness. The general trend for the most part is a monotonic reduction in postbuckling stiffness with increasing cutout size. The isotropic and the $[(0/90)_5]_s$ plates exhibit the largest losses in postbuckling stiffness for cutout sizes up to $d/W = 0.60$. The $[(\pm 45)_6]_s$ and $[(\pm 60)_6]_s$ plates with $d/W = 0.66$, which deform inelastically prior to buckling, exhibit the largest reductions in postbuckling stiffness. In contrast, the $[90_{10}]_s$ plates with $d/W = 0.21$, 0.32, and 0.42 exhibit postbuckling stiffnesses between 25 and 56 percent higher than the postbuckling stiffness of the corresponding plate without a cutout. The magnitude of these increases suggests that the increases in stiffness noted are not due entirely to scatter in the experimental data and suggest that further investigation of the importance of plate orthotropy on the postbuckling behavior of plates with cutouts should be performed. Moreover, these results suggest the possibility of tailoring the cutout size and the stacking sequence of a composite plate to optimize postbuckling stiffness.

The results presented in table 12 indicate the reduction in axial stiffness associated with changing from an unbuckled state to a buckled state as a function of cutout size and plate orthotropy. The stiffness changes presented in this table correspond to the percentage difference between the prebuckling stiffness and the initial postbuckling stiffness of each plate. The results presented in this table indicate that the isotropic plates lose between 35 and 40 percent of their stiffness due to buckling for the full range of cutout sizes. The specially orthotropic plates, however, have a much larger spread in the stiffness reductions with respect to the cutout sizes than the isotropic plates. The $[(\pm 60)_6]_s$ plates exhibit a trend similar to that of the isotropic plates (less than 6 percent variation) with the exception of the plate with $d/W = 0.66$. These plates deform inelastically prior to buckling. The largest stiffness reduction is exhibited by the $[0_{10}]_s$ plate without a cutout, and the smallest stiffness reduction is exhibited by the $[90_{10}]_s$ plate with $d/W = 0.21$.

Behavior of out-of-plane displacement field. Results showing the effects of cutout size and plate orthotropy on the shape of the out-of-plane displacement field (transverse deflection) are presented in figure 19 for $[0_{10}]_s$, $[(0/90)_5]_s$, $[90_{10}]_s$, and $[(\pm 60)_6]_s$ plates with $d/W = 0.11$, 0.32, 0.42, and 0.66. The out-of-plane displacement contours shown in this figure are photographs of moiré fringe patterns that were taken during testing and correspond to load levels that were well into the postbuckling range. The out-of-plane displacement patterns shown in the figure consist of one half-wave in both the length and width directions of the plate with the exception of the $[90_{10}]_s$ plate with $d/W = 0.11$. In this case, the displacement pattern consists of two half-waves along the plate length and one half-wave across the plate width.

The results shown in figure 19 indicate that cutout size and plate orthotropy have a pronounced effect on the distributions of the out-of-plane displacements of the plates. The results shown in figure 19(a) for the $[0_{10}]_s$ plate with $d/W = 0.11$ indicate that lines of constant out-of-plane displacement are somewhat oval in appearance but substantially elongated, with the longest axis of the oval being normal to the loading direction. The out-of-plane displacement distributions are typical of those that usually occur in a highly orthotropic plate. As the cutout size inceases, the out-of-plane displacement field redistributes to become more concentrated in the lateral regions of the plate near the unloaded edges, and fully envelops the full length of the plate.

The results shown in figure 19(b) for the $[(0/90)_5]_s$ plates (plates with a more moderate degree of orthotropy) indicate out-of-plane displacement patterns that are more evenly distributed than the displacement patterns of the $[0_{10}]_s$ plates. The displacement patterns shown for the $[(0/90)_5]_s$ plates with $d/W = 0.11$ and 0.42 are typical of an overall plate type of bending mode as opposed to a mode in which the out-of-plane displacement field becomes concentrated in the lateral regions of the plate near the unloaded edges. For the cutout size of $d/W = 0.66$, the out-of-plane displacement field in the $[(0/90)_5]_s$ plate also becomes concentrated in the lateral regions of the plate near the unloaded edges but not to the extent that is exhibited by the highly orthotropic $[0_{10}]_s$ plates. Results obtained for the isotropic plates and $[(\pm 30)_6]_s$ plates indicated behavior very similar to the behavior of the $[(0/90)_5]_s$ plates.

The results presented in figure 19(c) for the $[90_{10}]_s$ plates indicate out-of-plane displacement patterns that are evenly distributed. The results shown in figure 19(c) for the $[90_{10}]_s$ plate with $d/W = 0.66$ appear to be more evenly distributed over the plate than the corresponding results for the $[0_{10}]_s$ and $[(0/90)_5]_s$ plates, but in addition, the lines of constant out-of-plane displacement along the edges of the cutout appear to be more densely spaced.

The results presented in figure 19(d) for the $[(\pm 60)_6]_s$ plates indicate out-of-plane displacement patterns that are somewhat evenly distributed for the plates with $d/W = 0.11$ and 0.32. However, the results shown in figure 19(d) for the $[(\pm 60)_6]_s$ plate with $d/W = 0.66$ indicate that the out-of-plane displacement field is much more localized around the vicinity of the net section of the plate, unlike the out-of-plane displacement fields of the other plates with the large cutouts. This more localized distribution of the out-of-plane displacements may be related to the fact that the $[(\pm 60)_6]_s$ stacking sequence tends to relocate the inplane load outboard of the cutout much more than the isotropic, specially orthotropic, and $[(\pm 30)_6]_s$ plates relocate the inplane load. This more localized distribution of the out-of-plane displacements may also be related to the nonlinear (material) prebuckling deformations exhibited by this plate. The corresponding $[(\pm 45)_6]_s$ plates exhibited behavior very similar to the behavior of the $[(\pm 60)_6]_s$ plates.

Modal interaction. Another important topic briefly investigated in this paper that may be important in preliminary design of structures is the relationship between cutout size and modal interaction in plates. The results presented in figures 6, 7, 10, and 11 for the $[90_{10}]_s$ plates indicate that increasing the

cutout size can cause a buckling mode shape change to occur in a plate. For example, the $[90_{10}]_s$ plate without a cutout buckled into a mode that consisted of one half-wave normal to the loading direction and two half-waves in the loading direction, whereas the corresponding plate with $d/W = 0.21$ buckled into a mode that consisted of one half-wave in each direction. Moreover, the results show that a cutout size can exist for which a modal interaction occurs at the onset of buckling. Specifically, the $[90_{10}]_s$ plate with $d/W = 0.11$ exhibited an interaction between the mode shapes of the corresponding plates with $d/W = 0$ and $d/W = 0.21$. (See fig. 10.) None of the other 39 plates tested exhibited modal interaction at the onset of buckling.

Insight into the behavior of the plates with cutouts tested can be obtained by examining the buckling behavior of rectangular orthotropic plates that are simply supported on the unloaded edges, in accordance with the test fixture used in the experimental study. The standard plot of buckling coefficient K versus plate aspect ratio L/W found in most text books on stability of plates is composed of a series of curves, referred to as festooned curves, that intersect at cusps. Two examples are shown in figure 11. Each independent curve between cusps represents a specific buckling mode for a certain group of plate aspect ratios. As the plate aspect ratio increases past a certain value, the number of longitudinal half-waves in the buckling mode changes. Furthermore, at the cusps a unique buckling mode is indeterminant, since two distinct modes possess the same buckling load.

The location of these cusps is directly related to buckling behavior of the corresponding infinitely long plate. Analysis shows that the minimum points on the festooned curves occur at integer multiples of the aspect ratio of the repetitive buckle mode of the infinitely long plate. For other aspect ratios, the plate buckles at a higher load. This relationship accounts for the festooned nature of the curves of buckling load versus plate aspect ratio. The particular value of the aspect ratio of the buckling mode shape of the infinitely long plate is directly related to the inplane stresses acting in the plate, the boundary conditions acting on the unloaded edges, and the plate bending orthotropy. For the simply supported $[90_{10}]_s$ and $[0_{10}]_s$ plates without cutouts investigated in the present study, the aspect ratios of the buckling mode of infinitely long $[90_{10}]_s$ and $[0_{10}]_s$ plates are approximately 0.54 and 1.85, respectively. Thus, minimum points and cusps in a festooned curve plot of buckling coefficient versus plate aspect ratio are more closely spaced for $[90_{10}]_s$ plates than for $[0_{10}]_s$ plates. The close spacing of the cusps of the festooned curves of the $[90_{10}]_s$ plates and the close proximity of the first cusp to the unit plate aspect ratio (see fig. 11 for $d/W = 0$) indicate that a $[90_{10}]_s$ square plate is more likely to change buckle mode shape when a small perturbation in the buckle mode aspect ratio occurs than the other square plates investigated herein.

In a $[90_{10}]_s$ plate with $d/W = 0.11$, the cutout causes redistribution of the inplane prebuckling stresses and causes a decrease in bending stiffness in the central region of the plate. The decrease in bending stiffness results from the fact that material has been removed from the plate and from the fact that a free interior boundary is present. These effects (inplane and bending) associated with the cutout result in perturbing the aspect ratio of the buckle (or buckles) forming the mode shape and effectively shift the festooned curves until the first cusp is at a plate aspect ratio of 1, as indicated by the dashed line in figure 11. As the cutout size increases, the associated festooned curves shift more until the first cusp occurs at a plate aspect ratio significantly larger than 1. This observation accounts for the fact that the $[90_{10}]_s$ plates with $d/W > 0.11$ had buckle modes that consisted of one half-wave in each direction.

Analysis indicates that the other plates investigated in this study all possess festooned curves in which the first cusp, corresponding to a change in buckle pattern from one longitudinal half-wave to two half-waves, occurs at a plate aspect ratio substantially larger than 1. Specifically, the first cusp for these plates occurs at aspect ratios far enough removed from a value of 1 such that perturbations in the aspect ratio of the buckle mode due to cutout sizes as big as $d/W = 0.66$ do not cause a change in mode shape or a modal interaction at the onset of buckling. This observation accounts for the fact that the other 39 plates tested buckled into distinct mode shapes that consisted of one half-wave in each direction for the full range of cutout sizes. Analytical results supporting this discussion can be found in references 1 and 3 for specially orthotropic plates and symmetrically laminated angle-ply plates with cutouts, respectively. The results reported in these references, and results used to support the previous discussion, were obtained with the computer program described in reference 12.

Anomalous behavior. Results were obtained for the $[0_{10}]_s$ plate with $d/W = 0.32$ that indicated buckling behavior atypical of orthotropic plates. More specifically, the results presented in figures 4 and 5 for this plate indicate that the plate deforms initially in the direction of its geometric imperfection shape and then rapidly buckles into a similar mode shape in the opposite direction. During the testing of this plate, a snapping sound was

heard when the plate buckled. This observation is supported by the jump in the corresponding curve of load versus end-shortening shown in figure 4 and by the discontinuity in the corresponding curve load versus transverse deflection shown in figure 5. These results indicate that the onset of buckling occurred in a manner similar to a change in buckle pattern.

For this particular test specimen, it was found that the loaded edges of the specimen had not been properly machined which resulted in an eccentric loading. The eccentricity produced bending moments that increased in magnitude as the applied loading increased and acted to move the plate in the direction opposite to the geometric imperfection. Buckling occurred when these bending moments overcame the tendency of the plate to deform in the direction of its geometric imperfection.

Similar behavior was exhibited by the $[(0/90)_5]_s$ plate with $d/W = 0.66$. The curve of load versus transverse deflection shown in figure 9 for this case did not have a sharp discontinuity like that shown in figure 5 for the $[0_{10}]_s$ plate with $d/W = 0.32$. However, a jump is present in the curve of load versus end-shortening shown in figure 8 for the $[(0/90)_5]_s$ plate with $d/W = 0.66$, and a snapping sound was heard during the test when the plate buckled.

The curve of load versus transverse deflection shown in figure 17 for $[(\pm 45)_6]_s$ plate with $d/W = 0.32$ indicates that the plate also deformed initially in the direction of its geometric imperfection. However, no jump in the corresponding curve of load versus end-shortening (see fig. 16) is present, and no snapping sound was heard when the plate buckled. The absence of these effects may be associated with the nonlinear material behavior.

In the investigation of buckling and postbuckling behavior of asymmetrically laminated plates, such as the work reported in reference 13, the inherent mechanical coupling between membrane and bending action in the plate produces out-of-plane deformations as the applied axial loading increases in a manner similar to that associated with the load-path eccentricity previously described. The intensity of the prebuckling moments due to mechanical coupling, and the direction of the associated out-of-plane deformation, are determined by the plate stacking sequence. When the prebuckling moments produce out-of-plane deformations that act in a direction opposite to the plate's geometric imperfection, a snap-through buckling similar to that exhibited by the $[0_{10}]_s$ plate with $d/W = 0.32$ may occur. In such cases it is important to understand the two mechanisms, mechanical coupling (material induced eccentricity) and edge effects (geometry induced eccentricity), responsible for the plate behavior.

Concluding Remarks

An experimental study of the postbuckling behavior of square compression-loaded graphite-epoxy plates and isotropic plates with central circular cutouts has been presented. A wide range of cutout sizes and a broad spectrum of plate orthotropy has been investigated. Specifically, results have been presented for unidirectional $[0_{10}]_s$ and $[90_{10}]_s$ plates, $[(0/90)_5]_s$ plates, and for aluminum plates. Results have also been presented for $[(\pm\theta)_6]_s$ angle-ply plates for values of $\theta = 30°$, $45°$, and $60°$. The ratios of circular cutout diameter to plate width ranged from 0 to 0.66.

Experimental results have been presented that indicate that the change in axial stiffness of a plate at buckling is strongly dependent upon cutout size and plate orthotropy. The presence of a cutout gives rise to an internal load distribution that changes, sometimes dramatically, as a function of cutout size coupled with the plate orthotropy. Moreover, results that have been presented indicate that the reduction in prebuckling axial stiffness, associated with a cutout, is not generally equal to the reduction in cross-sectional area of the plate at the net section.

In the buckled state, the role of orthotropy increases to include bending in addition to membrane orthotropy. Experimental results indicate that most of the plates tested with cutouts exhibit less postbuckling stiffness than the corresponding plate without a cutout and that the amount of postbuckling stiffness generally decreases with increasing cutout size. However, the experimental results also indicate that some of the highly orthotropic plates with cutouts exhibit higher postbuckling stiffness than the corresponding plate without a cutout. In all these cases, the cutout size and plate orthotropy was found to dramatically affect the distribution of the out-of-plane displacement field that occurs in a buckled plate. These results suggest that the complex interaction of cutout size and orthotropy on the internal load distribution in plates needs further investigation. These results also suggest that the cutout size and the stacking sequence of a composite plate could be tailored to optimize postbuckling stiffness.

Experimental results also indicate that a cutout can influence modal interaction in a plate. Specifically, results show a plate with a relatively small cutout buckling at a higher load than the corresponding plate without a cutout due to modal interaction. Other results indicate the presence of nonlinear prebuckling deformations, due to material nonlinearity, in the angle-ply plates with $\theta = 45°$ and $60°$. The nonlinear prebuckling deformations are more pronounced in the plates with $\theta = 45°$, and become

even more pronounced as the cutout size increases. An important finding of this experimental study is that plates with large radius cutouts do exhibit some postbuckling strength.

NASA Langley Research Center
Hampton, VA 23665-5225
June 29, 1990

References

1. Nemeth, Michael Paul: Buckling Behavior of Orthotropic Composite Plates With Centrally Located Cutouts. Ph.D. Diss., Virginia Polytechnic Inst. & State Univ., May 1983.
2. Nemeth, Michael P.; Stein, Manuel; and Johnson, Eric R.: *An Approximate Buckling Analysis for Rectangular Orthotropic Plates With Centrally Located Cutouts.* NASA TP-2528, 1986.
3. Nemeth, Michael P.: Buckling Behavior of Compression-Loaded Symmetrically Laminated Angle-Ply Plates With Holes. *AIAA J.*, vol. 26, no. 3, Mar. 1988, pp. 330–336.
4. Yu, Wei-Wen; and Davis, Charles S.: Buckling Behavior and Post-Buckling Strength of Perforated Stiffened Compression Elements. *The First Specialty Conference on Cold Formed Steel Structures*, Wei-Wen Yu, ed., Civil Engineering Dept., Univ. of Missouri-Rolla 1971, pp. 58–64.
5. Martin, James: Buckling and Postbuckling of Laminated Composite Square Plates With Reinforced Central Circular Holes. Ph.D. Diss., Case Western Reserve Univ., 1972.
6. Yu, Wei-Wen; and Davis, Charles S.: Cold-Formed Steel Members With Perforated Elements. *J. Struct. Div., American Soc. Civ. Eng.*, vol. 99, no. ST10, Oct. 1973, pp. 2061–2077.
7. Ritchie, D.; and Rhodes, J.: Buckling and Post-Buckling Behavior of Plates With Holes. *Aeronaut. Q.*, vol. 26, pt. 4, Nov. 1975, pp. 281–296.
8. Starnes, James H., Jr.; and Rouse, Marshall: Postbuckling and Failure Characteristics of Selected Flat Rectangular Graphite-Epoxy Plates Loaded in Compression. *A Collection of Technical Papers – AIAA/ASME/ASCE/AHS 22nd Structures, Structural Dynamics & Materials Conference*, Part 1, Apr. 1981, pp. 423–434. (Available as AIAA-81-0543.)
9. Roberts, T. M.; and Azizian Z. G.: Strength of Perforated Plates Subjected to In-Plane Loading. *Thin-Walled Structures*, vol. 2, no. 2, 1984, pp. 153–164.
10. Narayanan, R.; and Chow, R. Y.: Ultimate Capacity of Uniaxially Compressed Perforated Plates. *Thin-Walled Structures*, vol. 2, no. 3, 1984, pp. 241–264.
11. VandenBrink, Dennis J.; and Kamat, Manohar P.: Post-Buckling Response of Isotropic and Laminated Composite Square Plates With Circular Holes. *Fifth International Conference on Composite Materials*, W. C. Harrigan, Jr., J. Strife, and A. K. Dhingra, eds., Metallurgical Soc., Inc., c.1985, pp. 1393–1409.
12. Nemeth, Michael P.: *A Buckling Analysis for Rectangular Orthotropic Plates With Centrally Located Cutouts.* NASA TM-86263, 1984.
13. Jensen, David W.; and Lagace, Paul A.: Influence of Mechanical Couplings on the Buckling and Postbuckling of Anisotropic Plates. *AIAA J.*, vol. 26, no. 10, Oct. 1988, pp. 1269–1277.

Table 1. Experimental Buckling Loads, Prebuckling Stiffnesses, and Initial Postbuckling Stiffnesses for Isotropic Plates

[All plates buckled into one half-wave along their length and width]

Specimen	d/W^a	Cutout diameter, in.	Buckling load, lb	Prebuckling stiffness, lb/in.	Initial postbuckling stiffness, lb/in.
A1	0	0	1872	541 139	329 201
A2	.10	.95	1828	477 341	309 093
A3	.20	1.90	1736	464 290	301 479
A4	.30	2.85	1656	426 445	277 715
A5	.40	3.80	1808	390 573	244 838
A6	.50	4.75	2007	326 186	204 760
A7	.60	5.70	1995	312 527	188 885

[a]Width equals distance between test fixture supports, 9.5 in.

Table 2. Experimental Buckling Loads, Prebuckling Stiffnesses, and Initial Postbuckling Stiffnesses for $[0_{10}]_s$ Laminates

[All plates buckled into one half-wave along their length and width]

Specimen	d/W^a	Cutout diameter, in.	Buckling load, lb	Prebuckling stiffness, lb/in.	Initial postbuckling stiffness, lb/in.
B1	0	0	9256	2 020 460	481 792
B2	.11	1.00	8975	1 473 710	487 362
B3	.21	2.00	8767	1 194 500	458 587
B4	.32	3.00	7689	1 266 500	494 835
B5	.42	4.00	6842	724 460	394 351
B6	.60	5.70	6464	641 878	376 653
B7	.66	6.25	6158	526 781	365 660

[a]Width equals distance between test fixture supports, 9.5 in.

Table 3. Experimental Buckling Loads, Prebuckling Stiffnesses, and Initial Postbuckling Stiffnesses for $[90_{10}]_s$ Laminates

[All plates buckled into one half-wave along their length and width unless otherwise noted]

Specimen	d/W[a]	Cutout diameter, in.	Buckling load, lb	Prebuckling stiffness, lb/in.	Initial postbuckling stiffness, lb/in.
C1	0	0	[b]2292	133 066	63 445
C2	.11	1.00	[c]294	132 428	61 114
C3	.21	2.00	2041	120 639	86 517
C4	.32	3.00	1690	125 131	79 401
C5	.42	4.00	1607	154 529	98 959
C6	.66	6.25	1868	60 955	36 444

[a]Width equals distance between test fixture supports, 9.5 in.
[b]Mode shape consists of two half-waves in the axial direction and one half-wave in the other direction.
[c]Mode shape influenced by modal interaction (see fig. 10).

Table 4. Experimental Buckling Loads, Prebuckling Stiffnesses, and Initial Postbuckling Stiffnesses for $[0/90_5]_s$ Laminates

[All plates buckled into one half-wave along their length and width]

Specimen	d/W[a]	Cutout diameter, in.	Buckling load, lb	Prebuckling stiffness, lb/in.	Initial postbuckling stiffness, lb/in.
D1	0	0	6950	955 427	447 631
D2	.11	1.00	6729	646 670	397 654
D3	.21	2.00	6407	586 874	391 869
D4	.32	3.00	6207	532 187	368 960
D5	.42	4.00	6510	535 595	330 118
D6	.60	5.70	6467	391 619	244 138
D7	.66	6.25	6581	370 703	220 011

[a]Width equals distance between test fixture supports, 9.5 in.

Table 5. Experimental Buckling Loads, Prebuckling Stiffnesses, and Initial Postbuckling Stiffnesses for $[(\pm 30)_6]_s$ Laminates

[All plates buckled into one half-wave along their length and width]

Specimen	d/W^a	Cutout diameter, in.	Buckling load, lb	Prebuckling stiffness, lb/in.	Initial postbuckling stiffness, lb/in.
E1	0	0	10 105	764 796	260 652
E2	.11	1.00	9 850	755 079	271 228
E3	.32	3.00	8 894	675 404	268 027
E4	.60	5.75	8 498	418 332	217 665
E5	.66	6.25	8 745	353 212	191 569

[a]Width equals distance between test fixture supports, 9.5 in.

Table 6. Experimental Buckling Loads, Prebuckling Stiffnesses, and Initial Postbuckling Stiffnesses for $[(\pm 60)_6]_s$ Laminates

[All plates buckled into one half-wave along their length and width unless otherwise noted]

Specimen	d/W^a	Cutout diameter, in.	Buckling load, lb	Prebuckling stiffness, lb/in.	Initial postbuckling stiffness, lb/in.
G1	0	0	5790	202 888	[b]122 920 (71 056)
G2	.11	1.00	5594	181 611	[b]121 305 (59 766)
G3	.32	3.00	4874	149 485	95 804
G4	.66	6.25	7107	[c]81 223 (62 189)	32 199

[a]Width equals distance between test fixture supports, 9.5 in.
[b]Postbuckling stiffness after change in buckle pattern to two half-waves along the loading axis.
[c]Tangent stiffness at the bifurcation point.

Table 7. Experimental Buckling Loads, Prebuckling Stiffnesses, and Initial Postbuckling Stiffnesses for $[(\pm 45)_6]_s$ Laminates

[All plates buckled into one half-wave along their length and width]

Specimen	d/W[a]	Cutout diameter, in.	Buckling load[b], lb	Prebuckling stiffness, lb/in.	Initial postbuckling stiffness, lb/in.
F1	0	0	9651	388 964	174 152
F2	.11	1.00	9188	317 706	174 016
F3	.32	3.00	8314	275 011	145 899
F4	.66	6.25	11 020	[c]145 951 (46 155)	46 155

[a]Width equals distance between test fixture supports, 9.5 in.
[b]Buckling loads estimated from out-of-plane displacements.
[c]Tangent stiffness at the bifurcation point.

Table 8. Analytic Buckling Loads, Critical End-Shortenings, and Nominal Thicknesses for Plates Without Cutouts

Plate type	Buckling load, P^o_{cr}, lb	Critical end-shortening Δ^o_{cr}, in.	Nominal thickness H, in.
Aluminum	1 773	0.002740	0.0647
$[0_{10}]_s$	9 272	.004556	.1100
$[90_{10}]_s$	2 473	.014050	.1100
$[(0/90)_5]_s$	6 544	.005875	.1100
$[(\pm 30)_6]_s$	9 898	.011759	.1176
$[(\pm 45)_6]_s$	10 962	.029268	.1300
$[(\pm 60)_6]_s$	5 944	.027752	.1176

Table 9. Failure Loads and Strains for $[90_{10}]_s$ and Angle-Ply Plates

	$[90_{10}]_s$		$[(\pm30)_6]_s$		$[(\pm60)_6]_s$		$[(\pm45)_6]_s$	
d/W^a	Failure load, lb	Average strain, Δ/L	Failure load, lb	Average strain, Δ/L	Failure load, lb	Average strain, Δ/L	Failure load, lb	Average strain, Δ/L
0.32	4028	0.004700						
.42	3247	.002800						
.60			12 895	0.00421				
.66	3412	.080382	12 080	.00424	8537	0.014148	12 601	0.015060

[a]Width equals distance between test fixture supports, 9.5 in.

Table 10. Reduction in Axial Prebuckling Stiffness Due to Cutout

	Reduction in axial prebuckling stiffness, percent						
		Specially orthotropic plates			Symmetrically laminated angle-ply plates		
d/W^a	Isotropic plates	$[0_{10}]_s$	$[90_{10}]_s$	$[(0/90)_5]_s$	$[(\pm30)_6]_s$	$[(\pm45)_60_s$	$[(\pm60)_6]_s$
0	0	0	0	0	0	0	0
.10	12						
.11		27	1	32	1	18	10
.20	14						
.21		41	9	39			
.30	21						
.32		37	6	44	12	29	26
.40	28						
.42		64	[b]−16	44			
.50	40						
.60	42	68		59	45		
.66		74	54	61	54	62	[c]60 (69)

[a]Width equals distance test fixture supports, 9.5 in.
[b]Minus sign represents increase in stiffness.
[c]Based on tangent stiffness at the bifurcation point.

Table 11. Change in Intial Postbuckling Stiffness Due to Cutout

d/W[b]	Change in postbuckling stiffness[a], percent						
	Isotropic plates	Specially orthotropic plates			Symmetrically laminated angle-ply plates		
		$[0_{10}]_s$	$[90_{10}]_s$	$[(0/90)_5]_s$	$[(\pm 30)_6]_s$	$[(\pm 45)_6]_s$	$[(\pm 60)_6]_s$
0	0	0	0	0	0	0	0
.10	−6						
.11		+1	−4	−11	+4	−1	−1
.20	−8						
.21		−5	+36	−12			
.30	−16						
.32		+3	+25	−18	+3	−16	−22
.40	−26						
.42		−18	+56	−26			
.50	−38						
.60	−43	−22		−45	−16		
.66		−24	−43	−51	−27	−73	−74

[a]Change in stiffness is with respect to the corresponding plate with $d/W = 0$. Negative values indicate reductions.
[b]Width equals distance between test fixture supports, 9.5 in.

Table 12. Reduction in Axial Stiffness in Going From Prebuckling State to Initial Buckled State

d/W[a]	Reduction in axial stiffness due to buckling, percent						
	Isotropic plates	Specially orthotropic plates			Symmetrically laminated angle-ply plates		
		$[0_{10}]_s$	$[90_{10}]_s$	$[(0/90)_5]_s$	$[(\pm 30)_6]_s$	$[(\pm 45)_6]_s$	$[(\pm 60)_6]_s$
0	39	76	52	53	66	55	39
.10	35						
.11		67	54	39	64	45	33
.20	35						
.21		62	28	33			
.30	35						
.32		61	37	31	60	47	36
.40	37						
.42		46	36	38			
.50	37						
.60	40	41		38	48		
.66		31	40	41	46	[b]68	[b]60

[a]Width equals distance between test fixture supports, 9.5 in.
[b]Includes material nonlinearity.

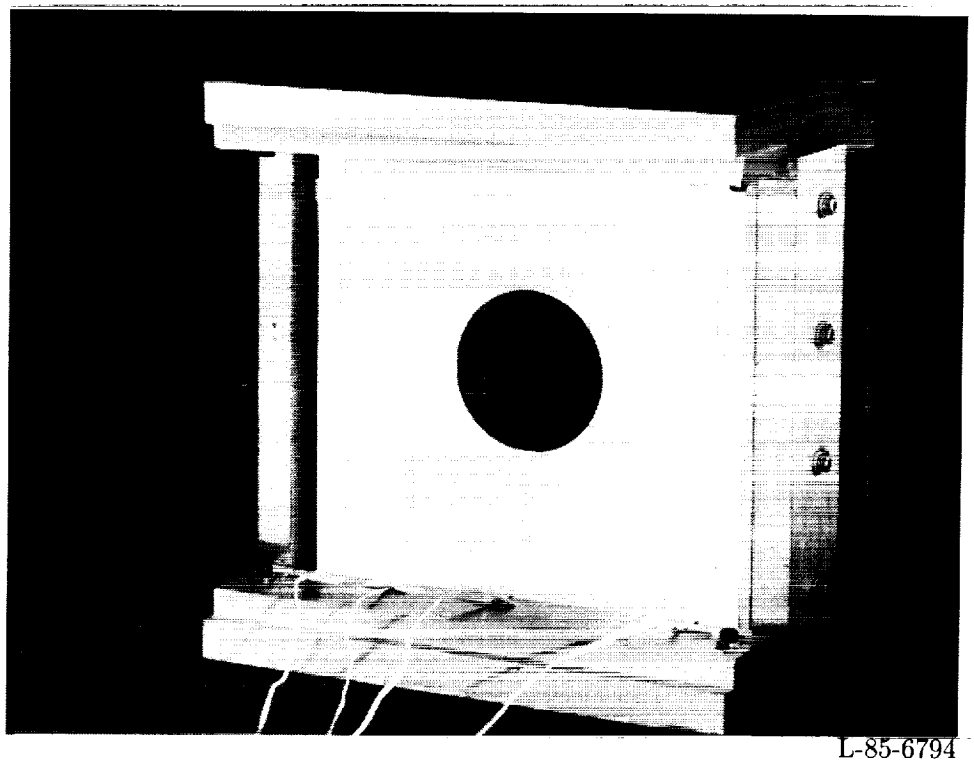

Figure 1. Specimen mounted in test fixture.

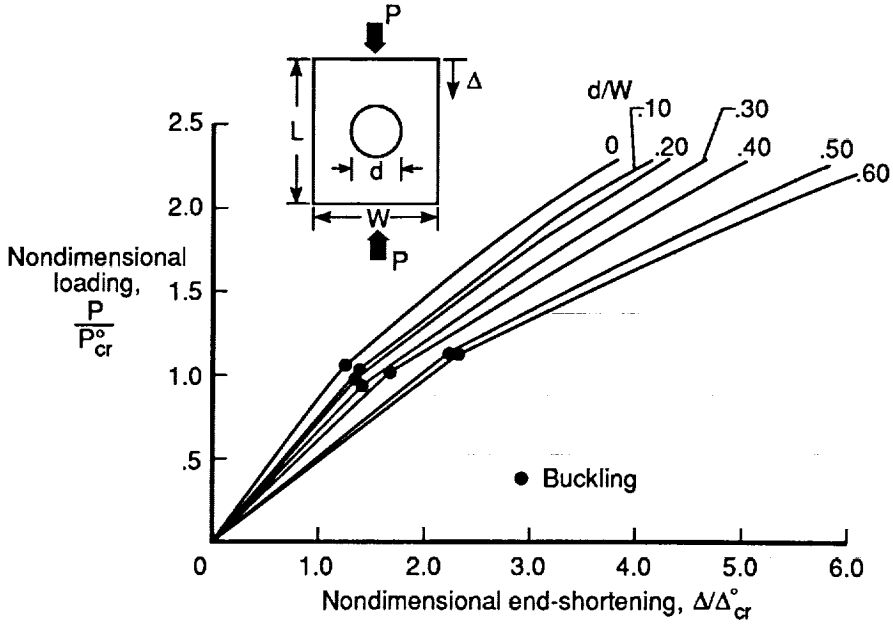

Figure 2. Nondimensional load versus end-shortening experimental results for isotropic square plates with central circular cutouts.

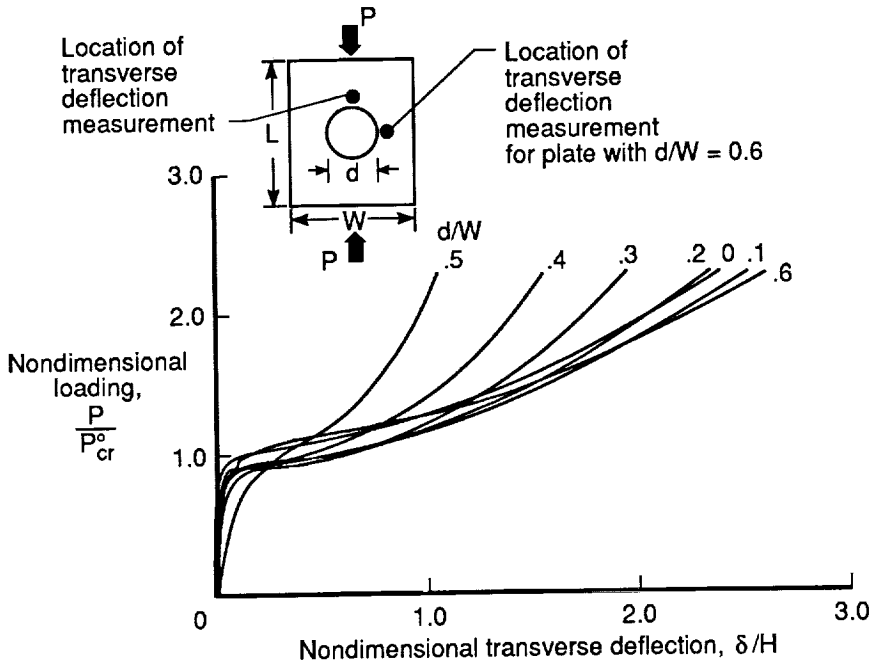

Figure 3. Nondimensional load versus transverse deflection experimental results for isotropic square plates with central circular cutouts.

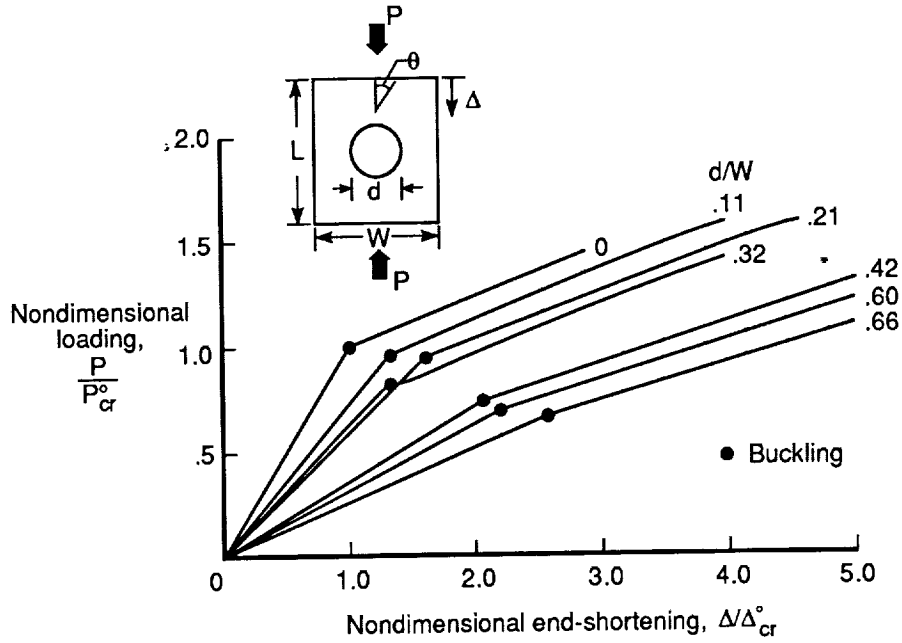

Figure 4. Nondimensional load versus end-shortening experimental results for $[0_{10}]_s$ square plates with central circular cutouts.

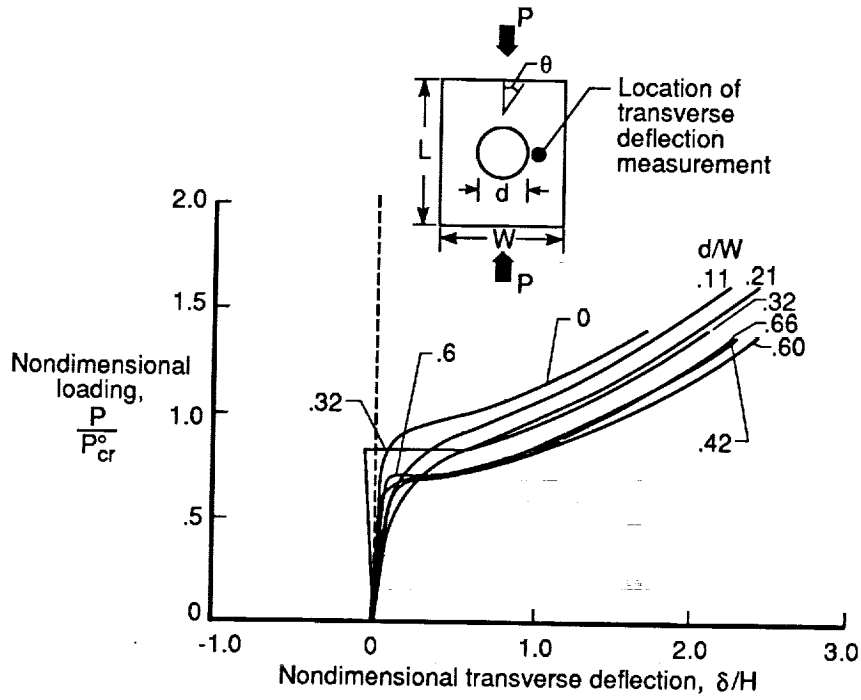

Figure 5. Nondimensional load versus transverse deflection experimental results for $[0_{10}]_s$ square plates with central circular cutouts.

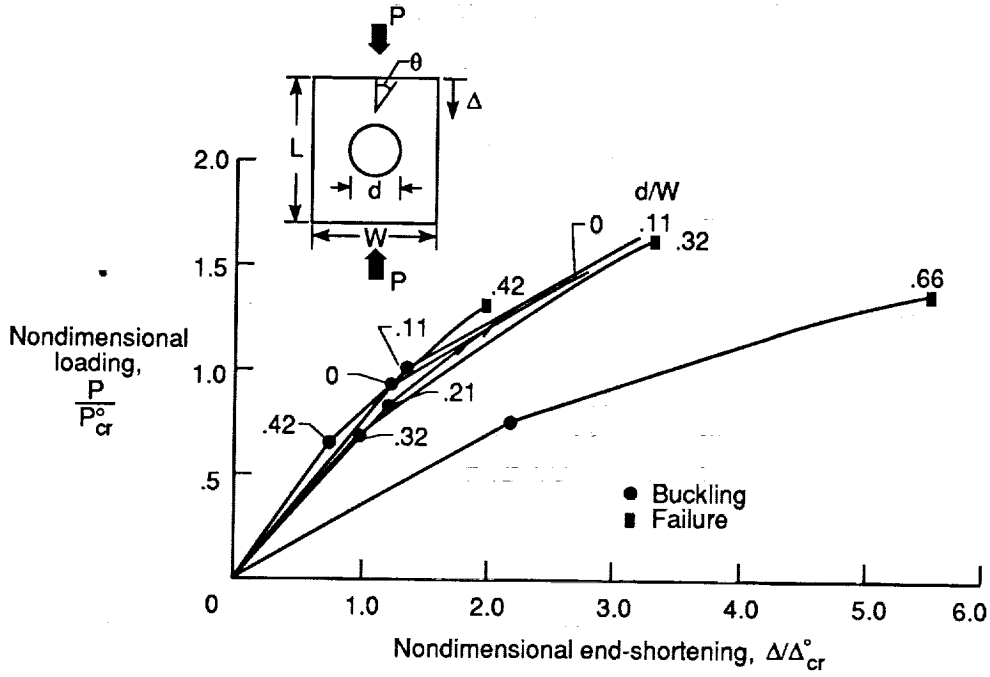

Figure 6. Nondimensional load versus end-shortening experimental results for $[90_{10}]_s$ square plates with central circular cutouts.

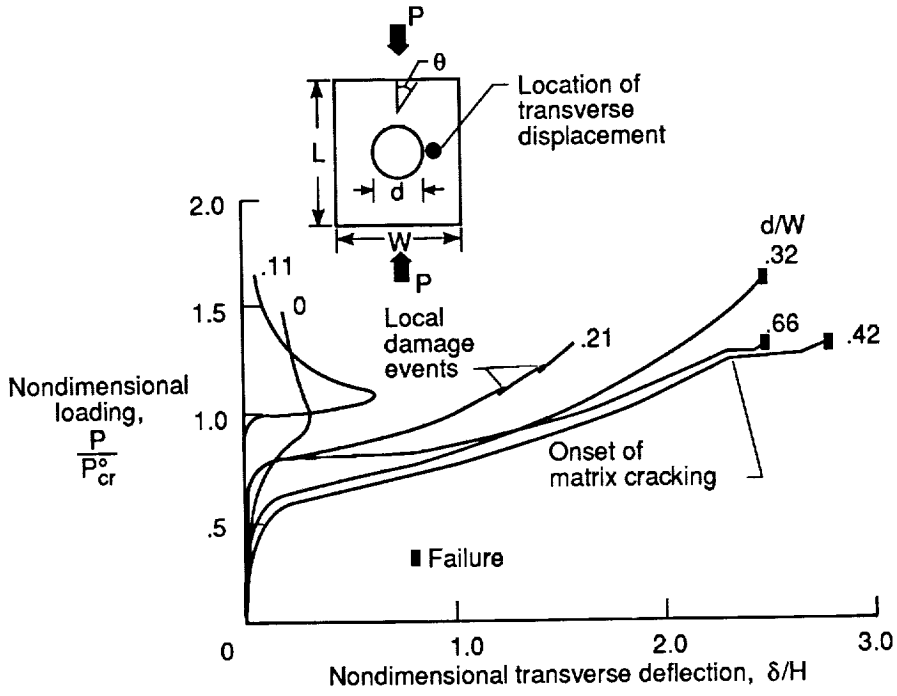

Figure 7. Nondimensional load versus transverse deflection experimental results for $[90_{10}]_s$ square plates with central circular cutouts.

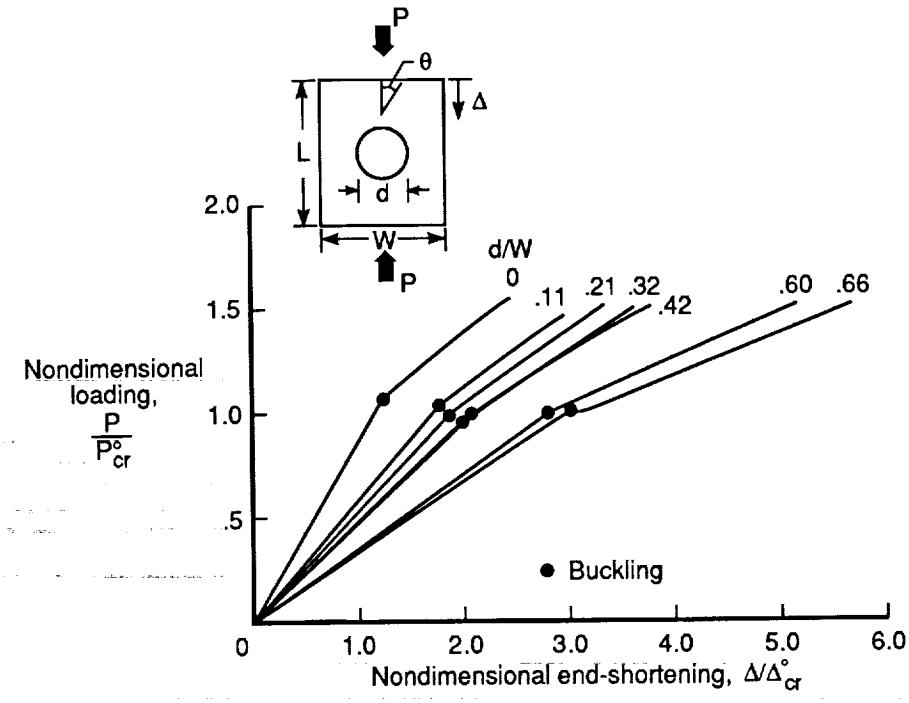

Figure 8. Nondimensional load versus end-shortening experimental results for $[(0/90)_5]_s$ square plates with central circular cutouts.

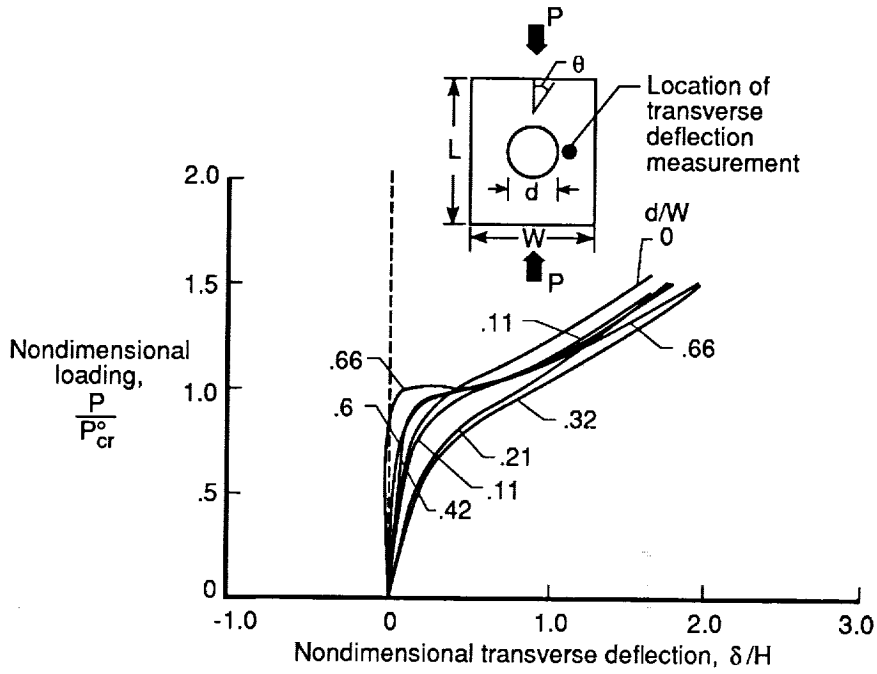

Figure 9. Nondimensional load versus transverse deflection experimental results for $[(0/90)_5]_s$ square plates with central circular cutouts.

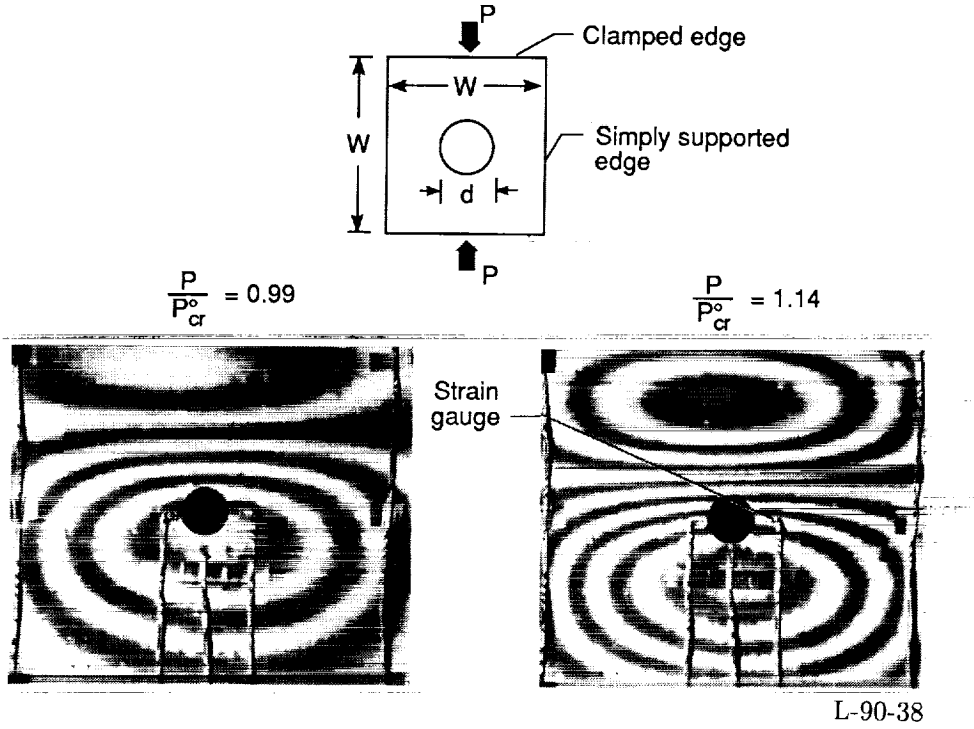

Figure 10. Interacting mode shapes for $[90_{10}]_s$ square plates with $d/W = 0.11$.

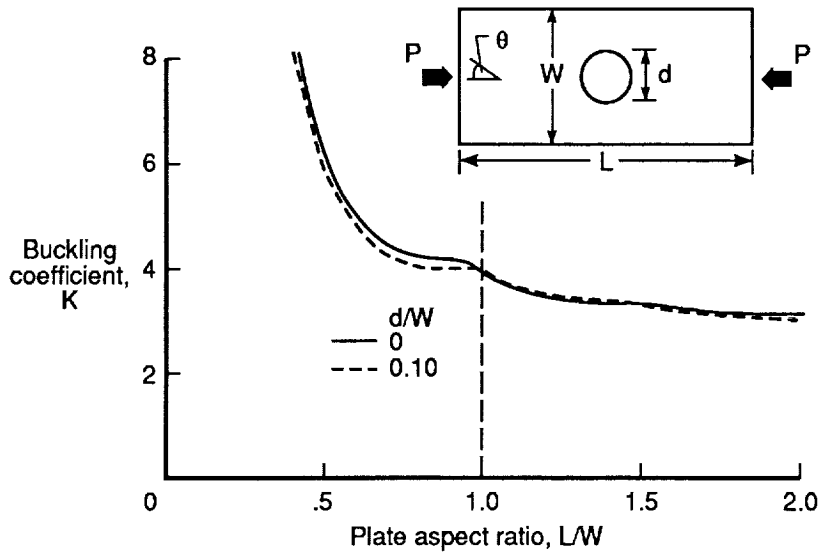

Figure 11. Buckling coefficients for $[90_{10}]_s$ rectangular plates with $d/W = 0$ and 0.10 (loaded edges clamped and unloaded edges simply supported).

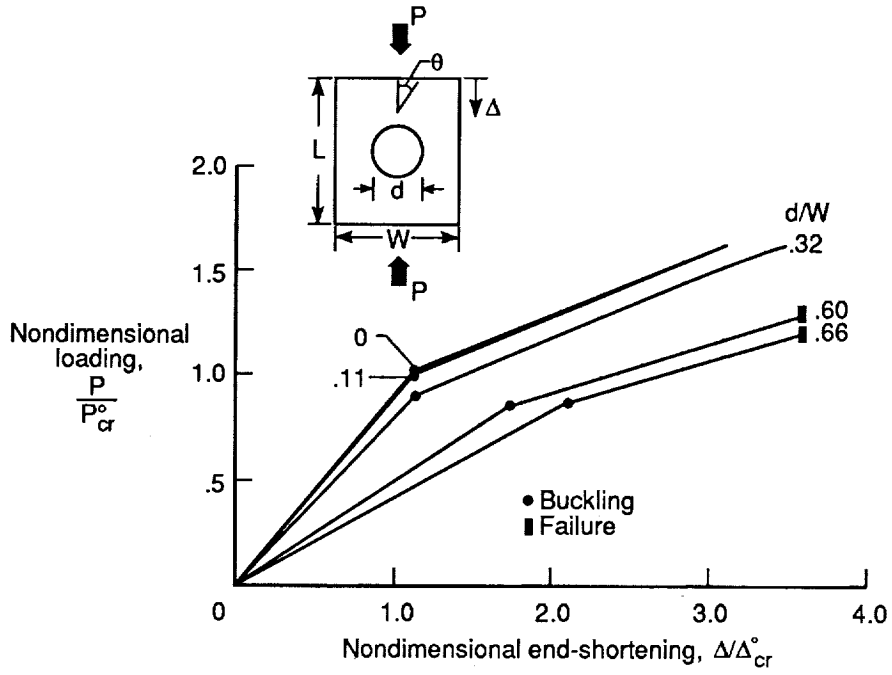

Figure 12. Nondimensional load versus end-shortening experimental results for $[(\pm 30)_6]_s$ square plates with central circular cutouts.

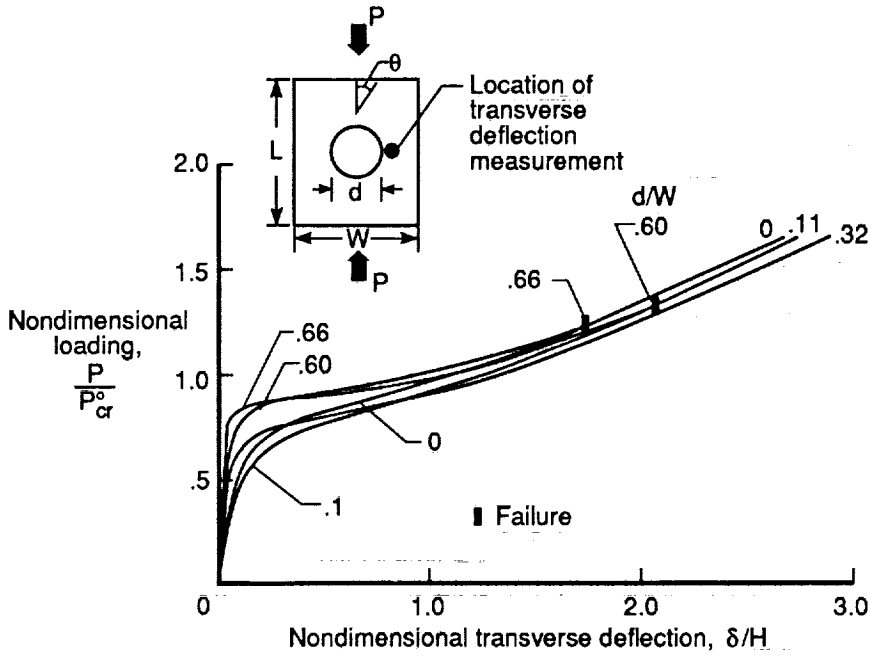

Figure 13. Nondimensional load versus transverse deflection experimental results for $[(\pm 30)_6]_s$ square plates with central circular cutouts.

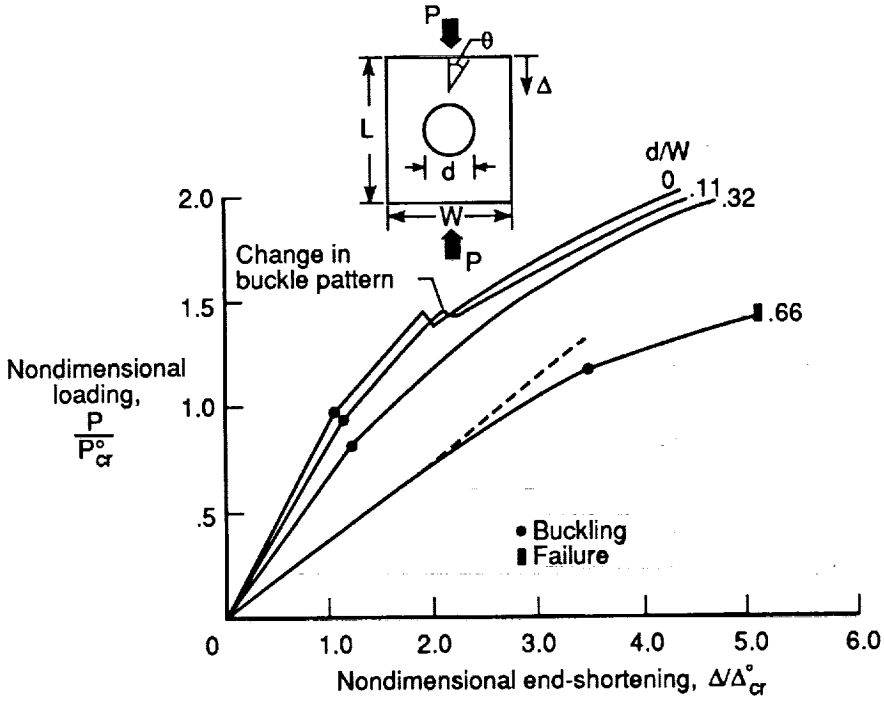

Figure 14. Nondimensional load versus end-shortening experimental results for $[(\pm 60)_6]_s$ square plates with central circular cutouts.

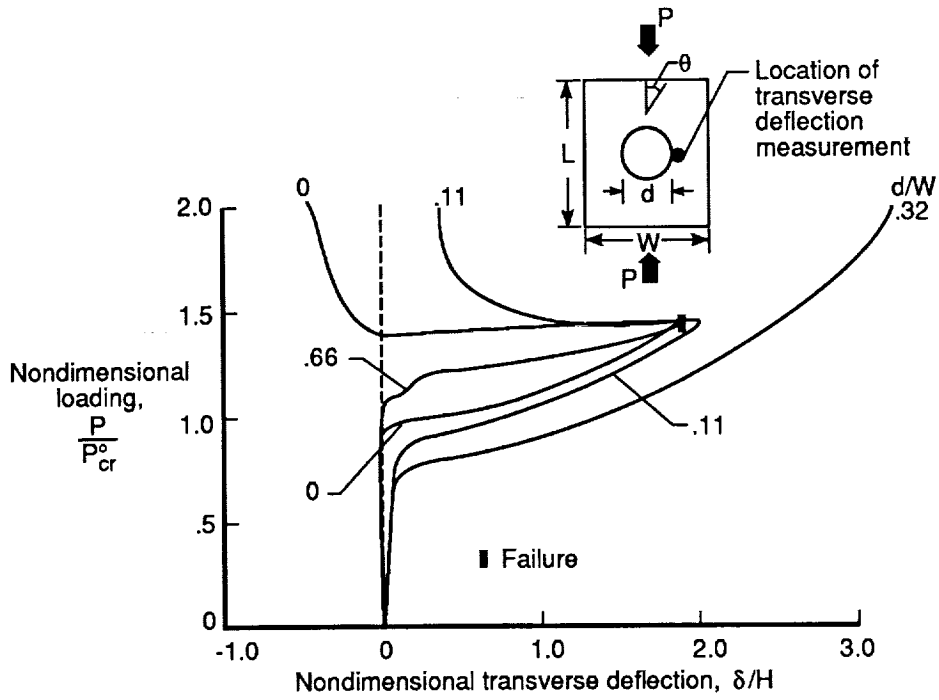

Figure 15. Nondimensional load versus transverse deflection experimental results for $[(\pm 60)_6]_s$ square plates with central circular cutouts.

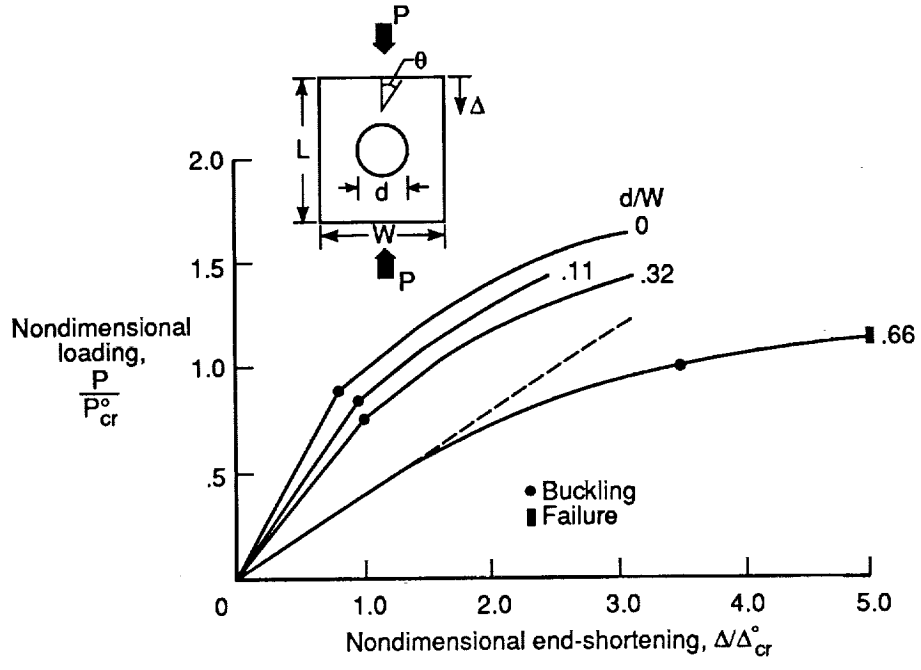

Figure 16. Nondimensional load versus end-shortening experimental results for $[(\pm 45)_6]_s$ square plates with central circular cutouts.

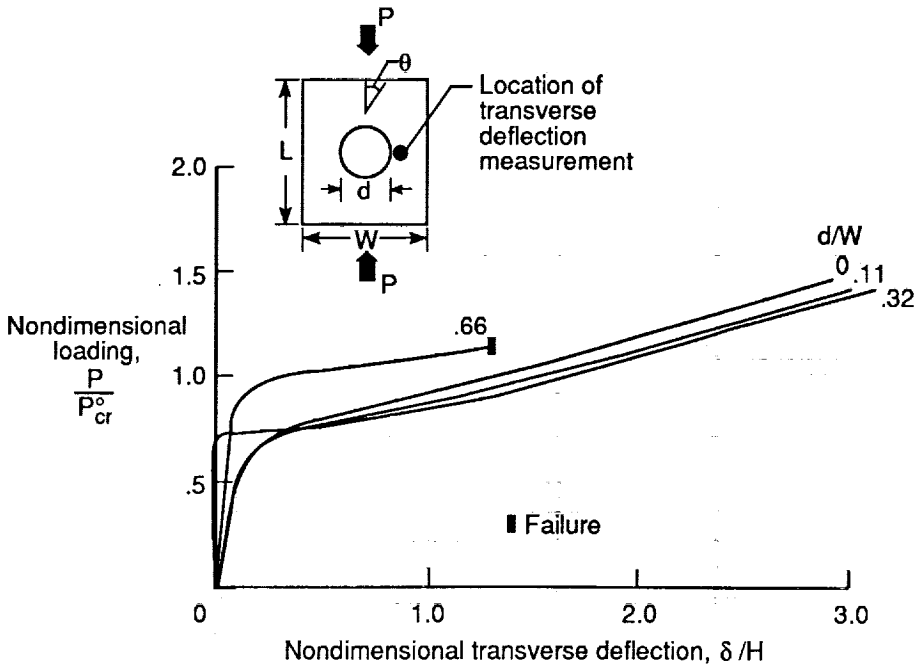

Figure 17. Nondimensional load versus transverse deflection experimental results for $[(\pm 45)_6]_s$ square plates with central circular cutouts.

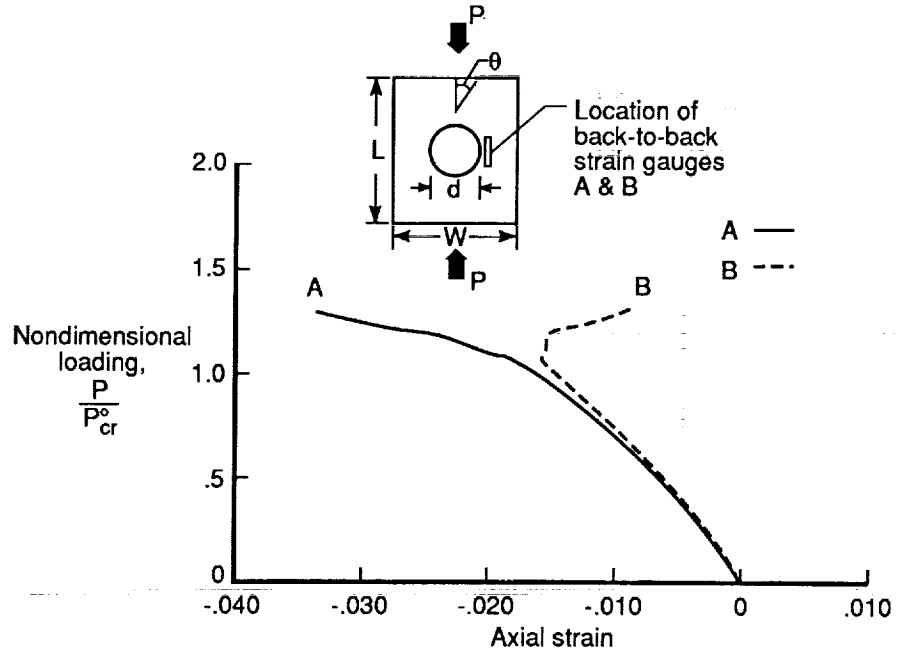

Figure 18. Strain near the cutout in the $[(\pm 60)_6]_s$ square plate with $d/W = 0.66$.

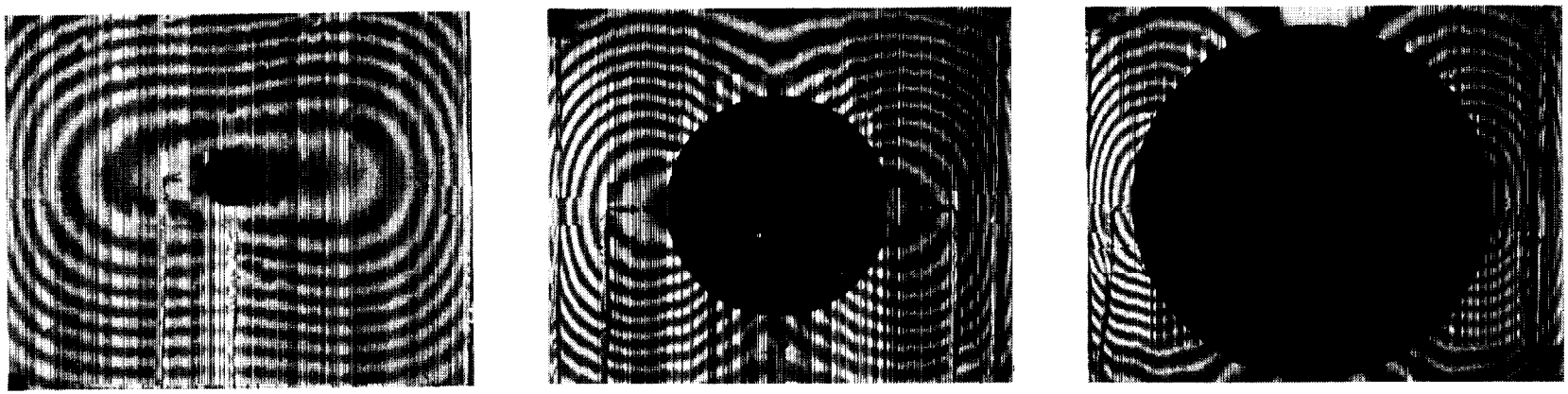

(a) Moiré fringe patterns of out-of-plane displacements for $[0_{10}]_s$ plates.

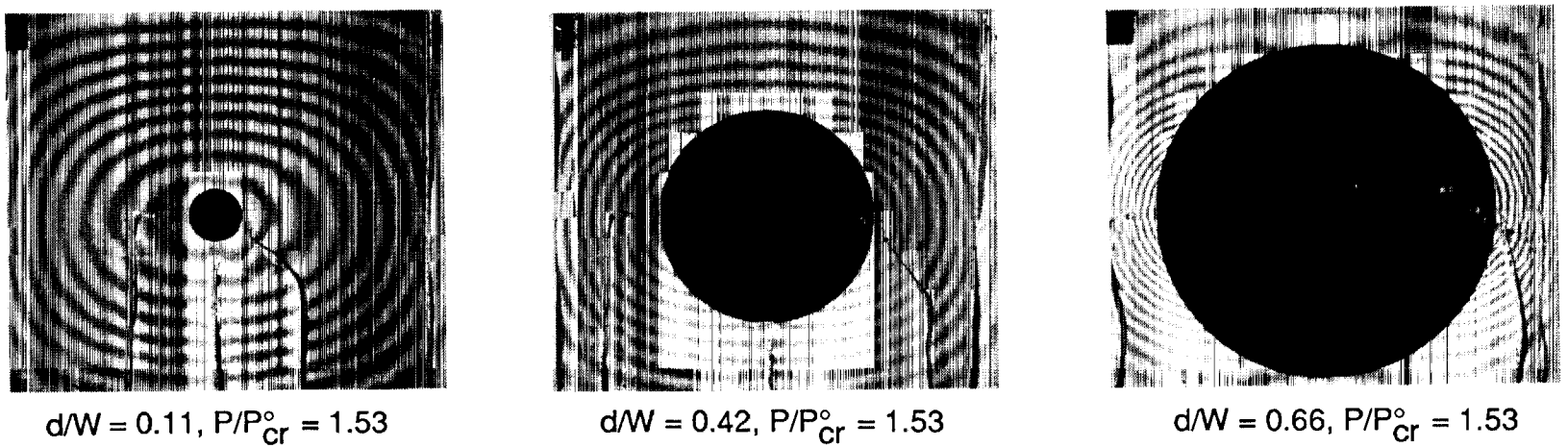

(b) Moiré fringe patterns of out-of-plane displacements for $[(0/90)_5]_s$ plates.

L-90-39

Figure 19. Out-of-plane displacement patterns for $[0_{10}]_s$, $[(0/90)_5]_s$, $[90_{10}]_s$, and $[(\pm 60)_6]_s$ square plates with central circular cutouts.

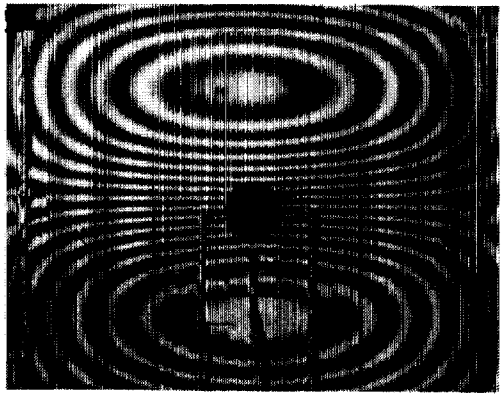

$d/W = 0.11, P/P^{\circ}_{cr} = 1.62$

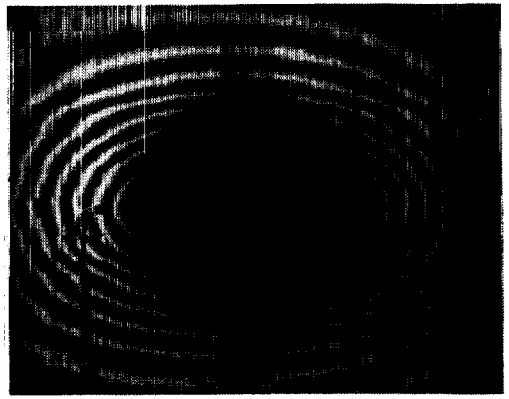

$d/W = 0.42, P/P^{\circ}_{cr} = 1.21$

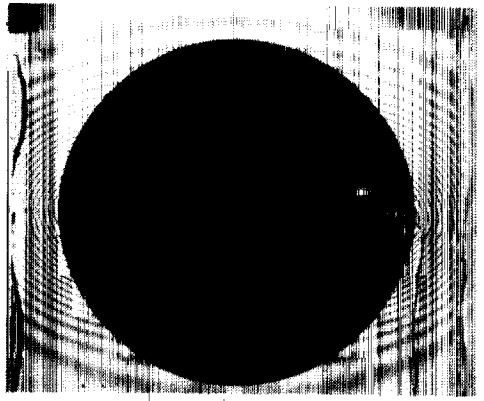

$d/W = 0.66, P/P^{\circ}_{cr} = 1.31$

(c) Moiré fringe patterns of out-of-plane displacements for $[90_{10}]_s$ plates.

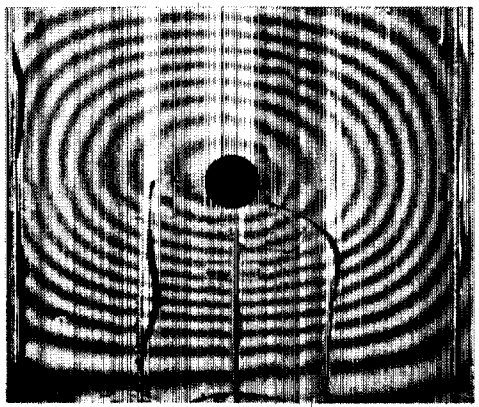

$d/W = 0.11, P/P^{\circ}_{cr} = 1.35$

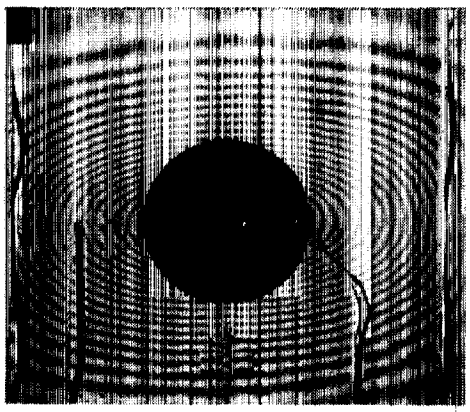

$d/W = 0.32, P/P^{\circ}_{cr} = 1.68$

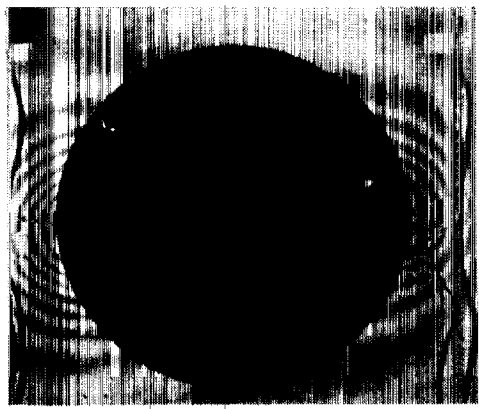

$d/W = 0.66, P/P^{\circ}_{cr} = 1.26$

(d) Moiré fringe patterns of out-of-plane displacements for $[(\pm 60)_6]_s$ plates.

L-90-40

Figure 19. Concluded.

NASA
National Aeronautics and Space Administration

Report Documentation Page

1. Report No.	2. Government Accession No.	3. Recipient's Catalog No.
NASA TP-3007		

4. Title and Subtitle	5. Report Date
Buckling and Postbuckling Behavior of Square Compression-Loaded Graphite-Epoxy Plates With Circular Cutouts	August 1990
	6. Performing Organization Code
7. Author(s)	8. Performing Organization Report No.
Michael P. Nemeth	L-16777
9. Performing Organization Name and Address	10. Work Unit No.
NASA Langley Research Center Hampton, VA 23665-5225	505-63-01-08
	11. Contract or Grant No.
12. Sponsoring Agency Name and Address	13. Type of Report and Period Covered
National Aeronautics and Space Administration Washington, DC 20546-0001	Technical Paper
	14. Sponsoring Agency Code

15. Supplementary Notes

Presented at the Eighth DoD/NASA/FAA Conference on Fibrous Composites in Structural Design, Norfolk, Virginia, November 28–30, 1989.

16. Abstract

An experimental study of the postbuckling behavior of square compression-loaded graphite-epoxy plates and isotropic plates with a central circular cutout is presented. Results are presented for unidirectional $[0_{10}]_s$ and $[90_{10}]_s$ plates, $[0/90_5]_s$ plates, and for aluminum plates. Results are also presented for $[(\pm\theta)_6]_s$ angle-ply plates for values of $\theta = 30°$, 45°, and 60°. The experimental results indicate that the change in axial stiffness of a plate at buckling is strongly dependent upon cutout size and plate orthotropy. The presence of a cutout gives rise to an internal load distribution that changes, sometimes dramatically, as a function of cutout size coupled with the plate orthotropy. In the buckled state, the role of orthotropy becomes more significant since bending in addition to membrane orthotropy is present. Most of the plates with cutouts exhibited less postbuckling stiffness than the corresponding plate without a cutout, and the postbuckling stiffness decreased with increasing cutout size. However, some of the highly orthotropic plates with cutouts exhibited more postbuckling stiffness than the corresponding plate without a cutout.

17. Key Words (Suggested by Authors(s))	18. Distribution Statement
Buckling Postbuckling Cutouts Compression loaded Composite plates	Unclassified—Unlimited Subject Category 24

19. Security Classif. (of this report)	20. Security Classif. (of this page)	21. No. of Pages	22. Price
Unclassified	Unclassified	31	A03

NASA FORM 1626 OCT 86 NASA-Langley, 1990

For sale by the National Technical Information Service, Springfield, Virginia 22161-2171